Massachusetts Institute of Technology

Extraction of spin-asymmetries in the production of exclusive π^+ with a longitudinally polarized target

Timothy B. Hayward, Harut Avakian, Maggie Kerr

March 11th, 2026

Nucleon Structure through Generalized Parton Distributions

- Generalized Parton Distributions (GPDs) unify form factors and parton distribution functions and provide a more complete 3D picture of the nucleus.
- Give access to information on the correlations between transverse position and longitudinal momentum of quarks and gluons inside the nucleus.
- Accessible experimentally through measurements of exclusive processes such as Deeply Virtual Compton Scattering (DVCS) or Deeply Virtual Meson Production (DVMP).

Nucleon Polarization	Quark Polarization: Unpolarized (U)	Quark Polarization: Longitudinally Polarized (L)	Quark Polarization: Transversely Polarized (T)
U	H		$\bar{E} = 2\tilde{H}_T + E_T$
L		$\widetilde{H}$	$\widetilde{E}_T$
T	E	$\widetilde{E}$	$H_T, \widetilde{H}_T$

Nucleon Tomography

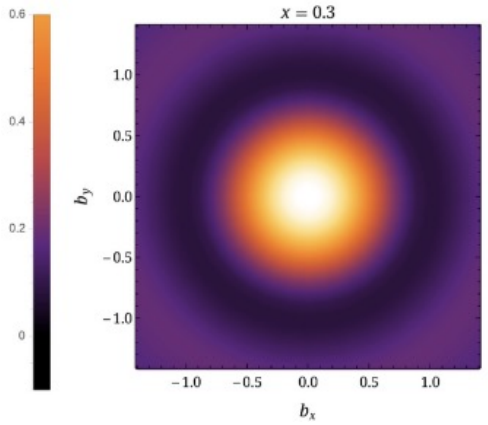

H.W. Lin, Phys. Rev. Lett. 127 (2021) 182001.

Contributions to the total nucleon spin

$$\frac{1}{2} = \frac{1}{2}\Delta\Sigma + \Delta L + \Delta G$$

X. Ji, Phys. Rev. Lett. 78,610 (1997)

1. Quark contribution; not the main contribution → spin crisis
2. Quark's orbital angular momentum, accessed through GPDs
3. Gluon spin contributions

Gravitational Form Factors

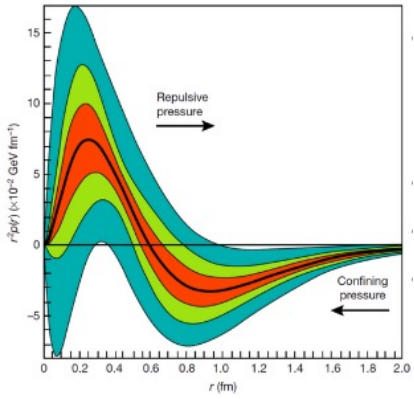

V. D. Burkert et al., Nature 557.7705 (2018): 396

- Mass/energy distribution inside the nucleon
- Nucleon mass radius
- Shear forces and pressure distributions

Nucleon Structure through (Chiral Odd) Generalized Parton Distributions

- Chiral odd GPDs encode how transversely polarized quark spins are distributed in position and momentum inside the nucleon and can be directly linked to the nucleon tensor charge and transverse-spin structure.
- Less experimentally constrained than chiral-even counterparts.
- Access to flavor dependence and unique isovector combinations not accessible in DVCS.

Nucleon Polarization	Quark Polarization: Unpolarized (U)	Quark Polarization: Longitudinally Polarized (L)	Quark Polarization: Transversely Polarized (T)
U	H		$\bar{E} = 2\tilde{H}_T + E_T$
L		$\widetilde{H}$	$\widetilde{E}_T$
T	E	$\widetilde{E}$	$H_T, \widetilde{H}_T$

Transversity Tomography

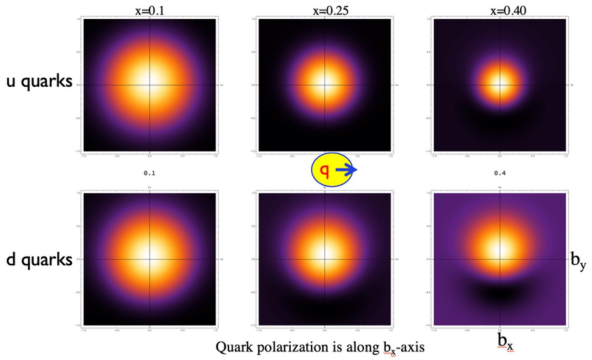

V. Kubarovsky, IWHSS/QCD-N 2025 (2025).

- Access to transversity/tensor charge
- Tensor charge is a key constraint in BSM searches (e.g. β decay, supersymmetry, leptoquarks etc.)

Flavor Separation

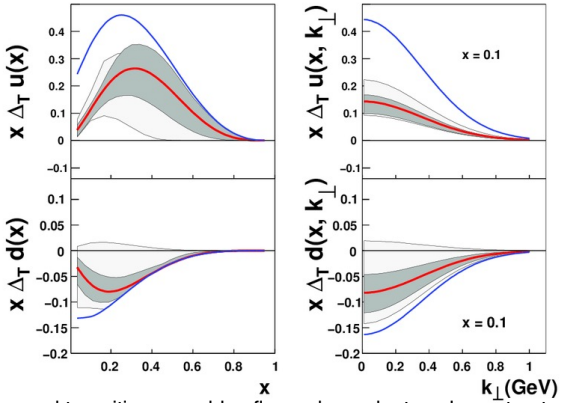

u → d transitions; enables flavor dependent nucleon structure

H. Gao, The European Physics Journal, Vol 126, 2 (2011).

Pion Cloud and Chiral Symmetry

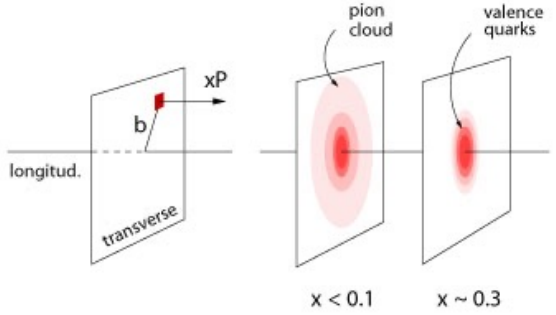

A. V. Belitsky and A. V. Radyushkin, Phys. Rept. 418 (2005) 1

- Access to the pion cloud through the pion pole term;
- Dependent on the pion-nucleon coupling and long-range structure of the nucleon (flavor asymmetry, nucleon charge radius, axial structure)

Run Group C Analysis

Period	Run Range	Beam Energy	FT	Torus	Solenoid	Coatjava Tracking	Beam Current
Su22	16043–16772	10.5473 GeV	On	−1	−1	10.0.9 (no DAF)	4 nA
Fa22	16843–17408	10.5473 GeV (16843–17065) 10.5563 GeV (17066–17408)	Off	−1	−1 (16843–17183) +1 (17185–17408)	11.1.0 (DAF)	8 nA
Sp23	17477–17811	10.5563 GeV (17477–17724) 10.5593 GeV (17725–17811)	On	−1 (17477–17768) +1 (17769–17811)	+1	11.1.0 (DAF)	4 nA

Period	Target	Total Charge (nC)	Share
Su22	NH3	3549857.7241	76.24%
	C	347844.3256	7.47%
	CH2	181529.4736	3.90%
	He	116142.5900	2.49%
	ET	460486.2692	9.89%
	Total	**4655860.3465**	
Fa22	NH3	5071114.4044	58.39%
	C	1729868.9114	19.92%
	CH2	1565074.5136	18.02%
	He	261852.4317	3.01%
	ET	57312.6648	0.66%
	Total	**8685222.9259**	
Sp23	NH3	998246.9959	45.43%
	C	331506.5461	15.09%
	CH2	431972.2728	19.68%
	He	264904.0752	12.05%
	ET	170812.0465	7.77%
	Total	**2197495.9365**	

- Make use of the full RGC inbending statistics (Su22, Fa22, Sp23).
- Dilution factor calculated via simultaneous measurements on C, CH_2, He-bath and empty target configurations.
- Target polarizations taken from combination of known A_{LL}s (elastic and DIS), P_b and D_f and solving for P_t.
- Comparison of data with both solenoid settings extensively studied with no impact on results observed.
- Leakage of tangentially polarized modulations into longitudinally polarized analysis studied with small impacts.

Dilution Factor Determination

Standalone dilution factor calculation by S.E. Kuhn and D. Holmberg.

NH/ND: Standard running with polarized e^- on the target cell filled with the polarized ammonia species of interest (NH_3 or ND_3). The total number of counts within a given bin $(\Delta Q^2, \Delta x, ...)$ and within cuts can be written as

$$N_A = X_A f_c \left[l_F \rho_F \Delta\sigma_F + (L - l_A)\rho_{He}\Delta\sigma_{He} + l_A \rho_A \left(\frac{7}{6}\Delta\sigma_C + 3\Delta\sigma_H \right) \right] \quad (3)$$

Contribution from Al foils

Contribution from He coolant

Contribution from nitrogen in ammonia

Contribution from hydrogen in ammonia

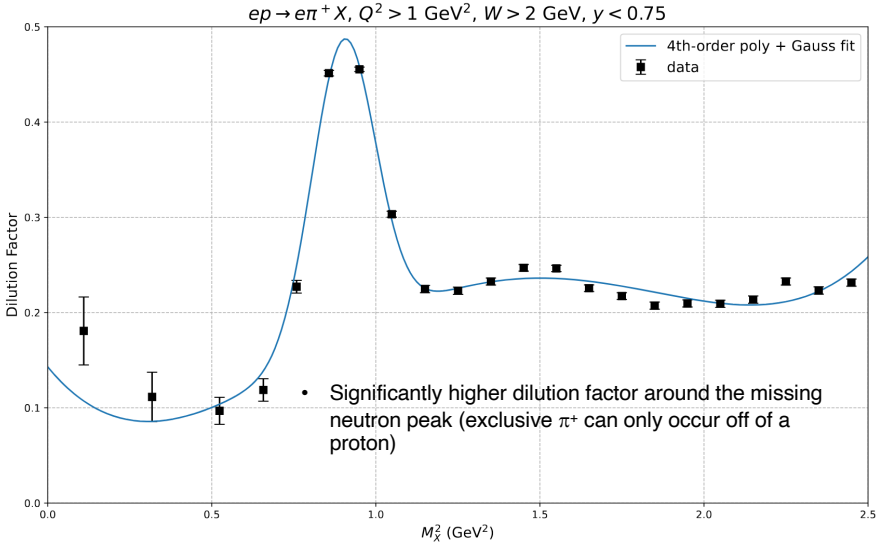

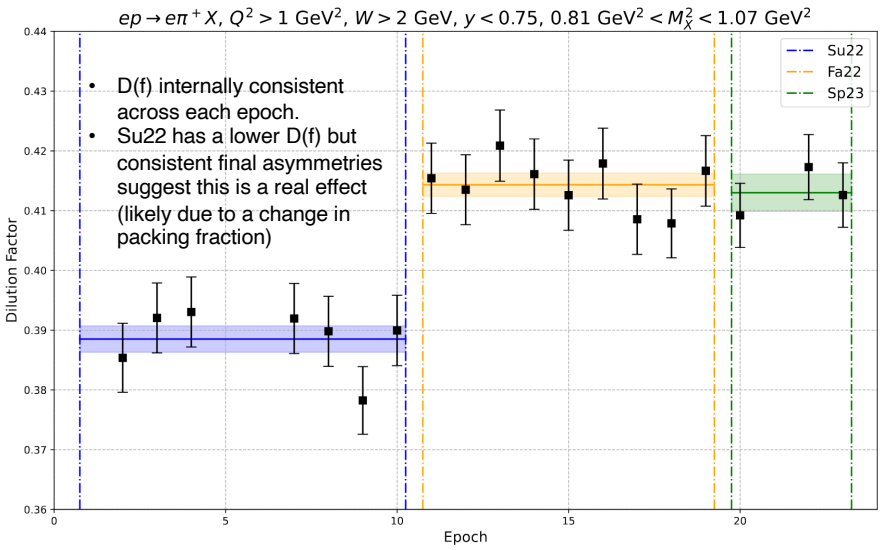

Asymmetry Extraction

In each kinematic bin we construct the three azimuthal asymmetries $A_{\mathrm{LU}}(\phi)$ (BSA), $A_{\mathrm{UL}}(\phi)$ (TSA), and $A_{\mathrm{LL}}(\phi)$ (DSA). The three channels are fit simultaneously using a common unpolarized denominator that carries the $\cos\phi$ and $\cos 2\phi$ modulations. Mean depolarization ratios evaluated in the bin,

$$R_{VA} \equiv \langle \mathrm{DepV} \rangle / \langle \mathrm{DepA} \rangle, \quad R_{BA} \equiv \langle \mathrm{DepB} \rangle / \langle \mathrm{DepA} \rangle, \quad R_{WA} \equiv \langle \mathrm{DepW} \rangle / \langle \mathrm{DepA} \rangle, \quad R_{CA} \equiv \langle \mathrm{DepC} \rangle / \langle \mathrm{DepA} \rangle,$$

are treated as fixed numbers and scale the corresponding harmonics. Defining the fit parameters (structure–function ratios)

$$\boldsymbol{p} = \left(C_{\mathrm{LU}},\, C_{\mathrm{UL}},\, A_{\mathrm{LU}}^{\sin\phi},\, A_{\mathrm{UL}}^{\sin\phi},\, A_{\mathrm{UL}}^{\sin 2\phi},\, A_{\mathrm{LL}},\, A_{\mathrm{LL}}^{\cos\phi},\, A_{\mathrm{UU}}^{\cos\phi},\, A_{\mathrm{UU}}^{\cos 2\phi}\right),$$

with $A_X^h \equiv F_X^h / F_{\mathrm{UU}}$, the shared denominator and the three model curves are

$$D(\phi) = 1 + R_{VA}\, A_{\mathrm{UU}}^{\cos\phi} \cos\phi + R_{BA}\, A_{\mathrm{UU}}^{\cos 2\phi} \cos 2\phi, \tag{1}$$

$$A_{\mathrm{LU}}^{\mathrm{model}}(\phi;\boldsymbol{p}) = C_{\mathrm{LU}} + \frac{R_{WA}\, A_{\mathrm{LU}}^{\sin\phi} \sin\phi}{D(\phi)}, \tag{2}$$

$$A_{\mathrm{UL}}^{\mathrm{model}}(\phi;\boldsymbol{p}) = C_{\mathrm{UL}} + \frac{R_{VA}\, A_{\mathrm{UL}}^{\sin\phi} \sin\phi + R_{BA}\, A_{\mathrm{UL}}^{\sin 2\phi} \sin 2\phi}{D(\phi)}, \tag{3}$$

$$A_{\mathrm{LL}}^{\mathrm{model}}(\phi;\boldsymbol{p}) = \frac{R_{CA}\, A_{\mathrm{LL}} + R_{WA}\, A_{\mathrm{LL}}^{\cos\phi} \cos\phi}{D(\phi)}, \tag{4}$$

where C_{LU} and C_{UL} absorb small offsets in LU and UL, respectively.

The χ^2 function is defined by letting $A_{\alpha,k}$ and $\sigma_{\alpha,k}$ denote the measured asymmetry and its statistical uncertainty in ϕ-bin k for channel $\alpha \in \{\mathrm{LU}, \mathrm{UL}, \mathrm{LL}\}$, evaluated at ϕ_k. The χ^2 function to be minimized in the simultaneous fit is then

$$\chi^2(\boldsymbol{p}) = \sum_k \frac{\left[A_{\mathrm{LU},k} - A_{\mathrm{LU}}^{\mathrm{model}}(\phi_k;\boldsymbol{p})\right]^2}{\sigma_{\mathrm{LU},k}^2} + \sum_k \frac{\left[A_{\mathrm{UL},k} - A_{\mathrm{UL}}^{\mathrm{model}}(\phi_k;\boldsymbol{p})\right]^2}{\sigma_{\mathrm{UL},k}^2} + \sum_k \frac{\left[A_{\mathrm{LL},k} - A_{\mathrm{LL}}^{\mathrm{model}}(\phi_k;\boldsymbol{p})\right]^2}{\sigma_{\mathrm{LL},k}^2}, \tag{5}$$

excluding any bins with vanishing $\sigma_{\alpha,k}$. All three sums share the same parameter vector $\boldsymbol{p}$, enforcing a common $\cos\phi$ and $\cos 2\phi$ denominator across the BSA, TSA and DSA.

Im(CFF)

BSA

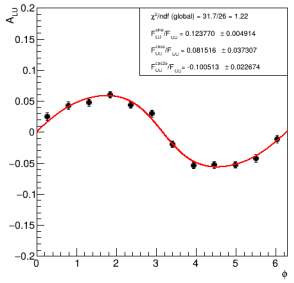

TSA

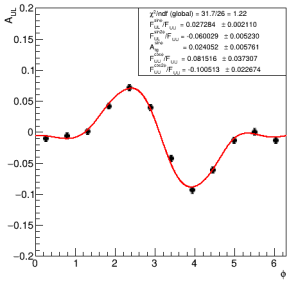

DSA

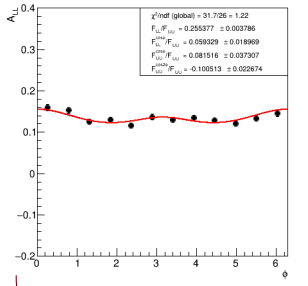

Re(CFF)

TL;DR: All five polarized modulations for BSA, TSA and DSA are extracted, with unpolarized modulations simultaneously constrained by all three histograms

Contribution from tangentially polarized terms

$$\sin\theta_\gamma = \gamma\sqrt{\frac{1-y-\frac{1}{4}y^2\gamma^2}{1+\gamma^2}}$$

- θ_γ defines the angle between the lepton beam-axis and the virtual-photon direction.
- Because the target is longitudinally polarized along the beam it is not completely longitudinally polarized along the direction **q** of the virtual photon.

$$S_\parallel^\gamma = P_t\cos\theta_\gamma \quad |\vec{S}_T^\gamma| = P_t\sin\theta_\gamma$$

- Any non-vanishing tangential polarization can produce UT-type modulations

$$A_{UT}^{\sin\phi}\sin\phi$$

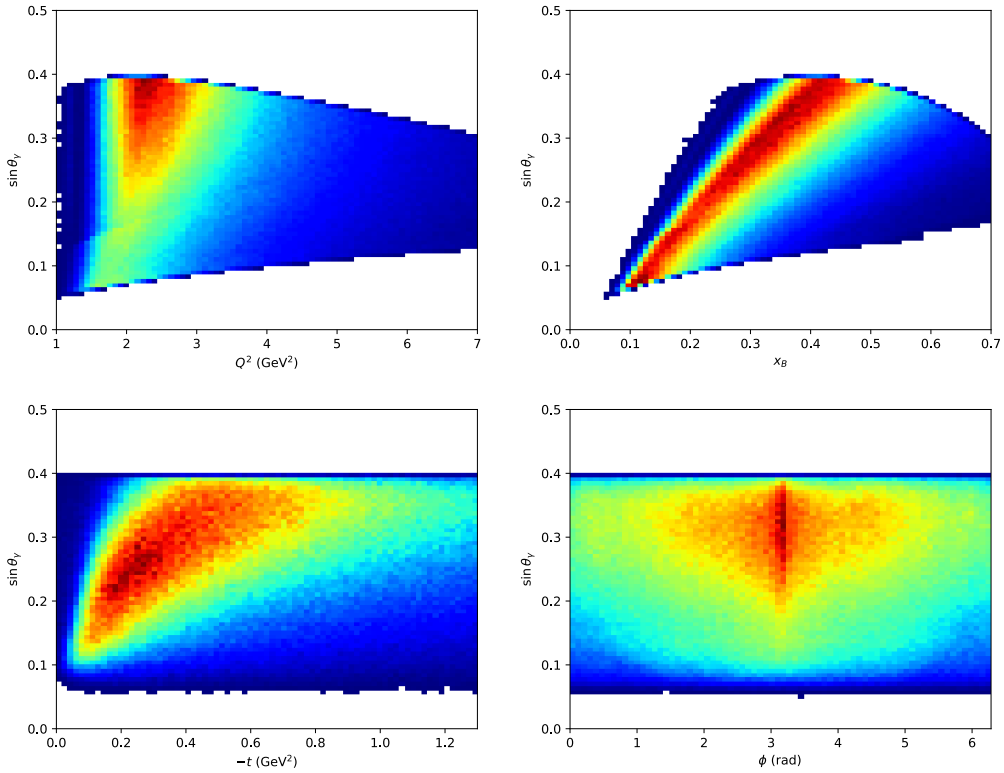

Introduction of "A_{UT}"

- If a $\sin(\theta_\gamma)$ $A_{UT}\sin(\phi)$ term is included directly it will be nearly collinear with the ordinary $\sin(\phi)$ basis.

$$m_i(\phi) \equiv \langle \sin\theta_\gamma \rangle_{\phi_i}$$

$$A_{UL}^{\sin\phi}\sin\phi + A_{UL}^{\sin 2\phi}\sin 2\phi \rightarrow A_{UL}^{\sin\phi}\sin\phi + A_{tg}m_i(\phi)\sin\phi + A_{UL}^{\sin 2\phi}\sin 2\phi$$

$$= \left[A_{UL}^{\sin\phi} + A_{tg}m_i(\phi)\right]\sin\phi + A_{UL}^{\sin 2\phi}\sin 2\phi$$

$$m(\phi) \equiv \overline{m} + \delta_m(\phi)$$

- Compute weighted mean and charge weighted width of distribution $\overline{m} = \frac{\sum_i w_i m_i}{\sum w_i}; \quad \sigma_w^2 = \frac{\sum_i w_i (m_i - \overline{m})^2}{\sum_i w_i}$
- Define the centered unitless shape $m_i^c(\phi) = \frac{\delta_m(\phi)}{\sigma_w}; \quad m_i^c(\phi) \equiv \frac{m_i(\phi) - \overline{m}}{\sigma_w}; \quad m_i(\phi) = \overline{m} + \sigma_w m_i^c(\phi)$
- First term renormalizes the $A_{UL}\sin(\phi)$ amplitude, second term carries the genuine shape of the "A_{tg}"
- Rewrite original modulation $m_i(\phi)\sin\phi = [\overline{m} + \sigma_w m_i^c(\phi)]\sin\phi$
- Plug back into TSA $A_{UL}^{\sin\phi}\sin\phi + A_{tg}m_i\sin\phi + A_{UL}^{\sin 2\phi}\sin 2\phi = A_{UL}^{\sin\phi} + A_{tg}\left[\overline{m} + \sigma_w m_i^c(\phi)\right]\sin\phi$

$$= \left[A_{UL}^{\sin\phi} + A_{tg}\overline{m}\right]\sin\phi + A_{tg}\sigma_w m_i^c(\phi)\sin\phi + A_{UL}^{\sin 2\phi}\sin 2\phi$$

Additional ϕ shape from m(ϕ)

- $\sin\theta_\gamma$ generally increases at the edges of ϕ bins.
- If $\sin\theta_\gamma$ had been ϕ-independent there would be no additional modulation effect from the tangential polarization.
- Magnitude of the information about A_{tg} is set by the σ_w (~2-3%).
- If A_{tg} is not fit, A_{UL} shifts by $\overline{m}A_{tg}$

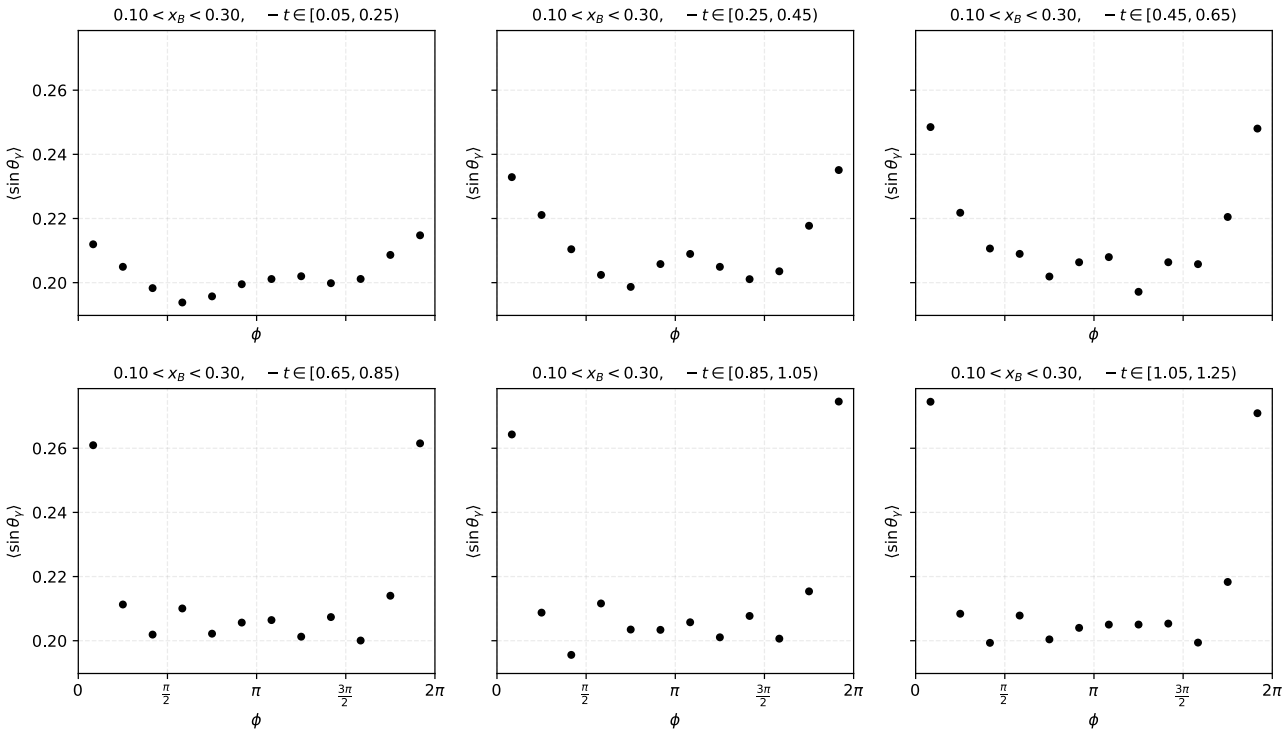

Fits including A_{tg} in TSA

- When included in the fit a small, possibly positive, contribution appears for the A_{tg} term.
- Little to no effect on the regular A_{UL} amplitudes.
- For $\langle \sin\theta_\gamma \rangle \sim 0.23$ and $A_{tg} \sim 0.03$ then $\Delta A_{UL} \sim 0.007$, i.e. a percent effect on the total magnitude.

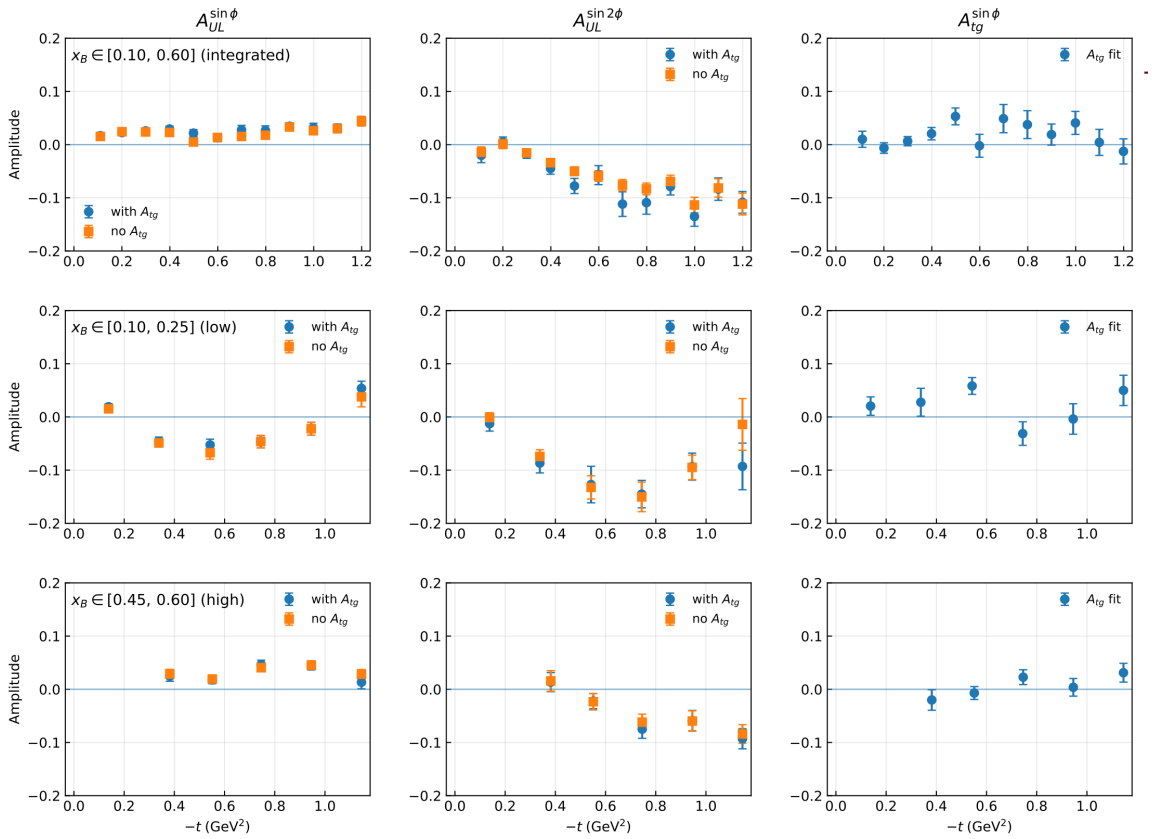

BSA

Goloskokov & Kroll, Eur. Phys. J. C **65** (2010) 137; [arXiv:0906.0460]

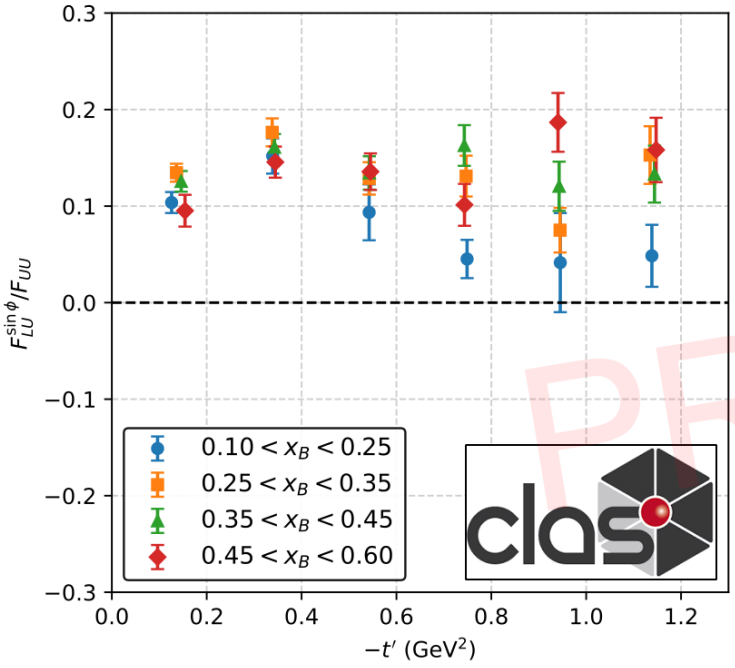

$$A_{LU}^{\sin\phi}\,\sigma_0^M = e_0^2\sqrt{1-\xi^2}\,\frac{\sqrt{-t'}}{2m}\,\mathrm{Im}\Big\{\Big[(1+\eta_M)\,\langle\bar{E}_T^M\rangle_{TL}^* + (1-\eta_M)\,\langle E_T^M\rangle_{TL}^*\Big]\,\langle H_{\rm eff}^M\rangle_{LL}$$

$$+\left[\frac{t'}{2m^2}(1+\eta_M)\,\langle\tilde{H}_T^M\rangle_{TL}^* - 2\,\langle H_T^M\rangle_{TL}^* + \frac{2\xi}{1-\xi^2}\,\langle E_T^M\rangle_{TL}^*\right]\langle E^M\rangle_{LL}\Big\}, \qquad (1)$$

η_M = -1 for pseudoscalar mesons

$$A_{LU}^{\sin\phi}\,\sigma_0^M = e_0^2\sqrt{1-\xi^2}\,\frac{\sqrt{-t'}}{2m}\,\mathrm{Im}\Big\{\underbrace{2\,\langle E_T^M\rangle_{TL}^*}_{3}\,\underbrace{\langle H_{\rm eff}^M\rangle_{LL}}_{1} + \Big[\underbrace{-2\,\langle H_T^M\rangle_{TL}^*}_{4} + \frac{2\xi}{1-\xi^2}\,\underbrace{\langle E_T^M\rangle_{TL}^*}_{3}\Big]\,\underbrace{\langle E^M\rangle_{LL}}_{2}\Big\}, \qquad (3)$$

1) Helicity-conserving longitudinal amplitude built primarily from $\tilde{H}^M$, encodes the quark helicity transverse distribution
2) Nucleon helicity-flip longitudinal amplitude built from $\tilde{\mathcal{E}}^M$; describes how axial charge (helicity density) is displaced when the nucleon flips its spin
3) Describes the transverse shift of quarks with a given transverse spin inside an unpolarized nucleon, analogous to sideways shift from Sivers
4) Generalized transversity GPD (reduces to $h_1(x)$ in the forward limit), encodes information on the correlation between transversely-polarized quarks in a transversely-polarized nucleon

Twist-3 TSA

Goloskokov & Kroll, Eur. Phys. J. C **65** (2010) 137; [arXiv:0906.0460]

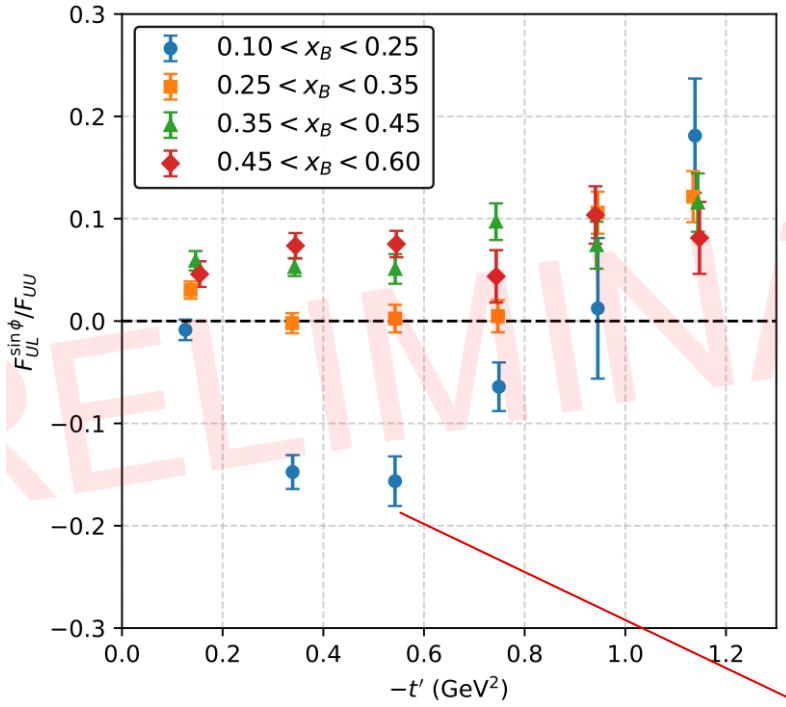

$$A_{UL}^{\sin\phi}\,\sigma_0^M = e_0^2\sqrt{1-\xi^2}\,\frac{\sqrt{-t'}}{2m}\,\mathrm{Im}\Big\{\Big[(1-\eta_M)\,\langle\overline{E}_T^M\rangle_{TL}^* + (1+\eta_M)\,\langle E_T^M\rangle_{TL}^*\Big]\langle H_{\rm eff}^M\rangle_{LL}$$

$$+\left[\frac{t'}{2m^2}(1-\eta_M)\,\langle\tilde{H}_T^M\rangle_{TL}^* - 2\,\langle H_T^M\rangle_{TL}^* + \frac{2\xi}{1-\xi^2}\,\langle E_T^M\rangle_{TL}^*\right]\langle E^M\rangle_{LL}\Big\}. \qquad (2)$$

η_M = -1 for pseudoscalar mesons

$$A_{UL}^{\sin\phi}\,\sigma_0^M = e_0^2\sqrt{1-\xi^2}\,\frac{\sqrt{-t'}}{2m}\,\mathrm{Im}\Big\{2\,\underbrace{\langle\overline{E}_T^M\rangle_{TL}^*}_{6}\,\underbrace{\langle H_{\rm eff}^M\rangle_{LL}}_{1} + \Big[\underbrace{\frac{t'}{m^2}\,\langle\tilde{H}_T^M\rangle_{TL}^*}_{5} - 2\,\underbrace{\langle H_T^M\rangle_{TL}^*}_{4} + \frac{2\xi}{1-\xi^2}\,\underbrace{\langle E_T^M\rangle_{TL}^*}_{3}\Big]\,\underbrace{\langle E^M\rangle_{LL}}_{2}\Big\}.$$

(4)

5) Partner to H_T, akin to pretzelosity, associated with quadrupole deformation in the distribution of quark transverse spin when the nucleon is transversely polarized

6) $\overline{E} = 2\tilde{H}_T + E_T$

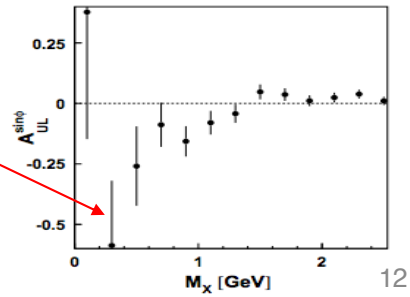

TT Interference

Goloskokov & Kroll, Eur. Phys. J. C **65** (2010) 137; [arXiv:0906.0460]

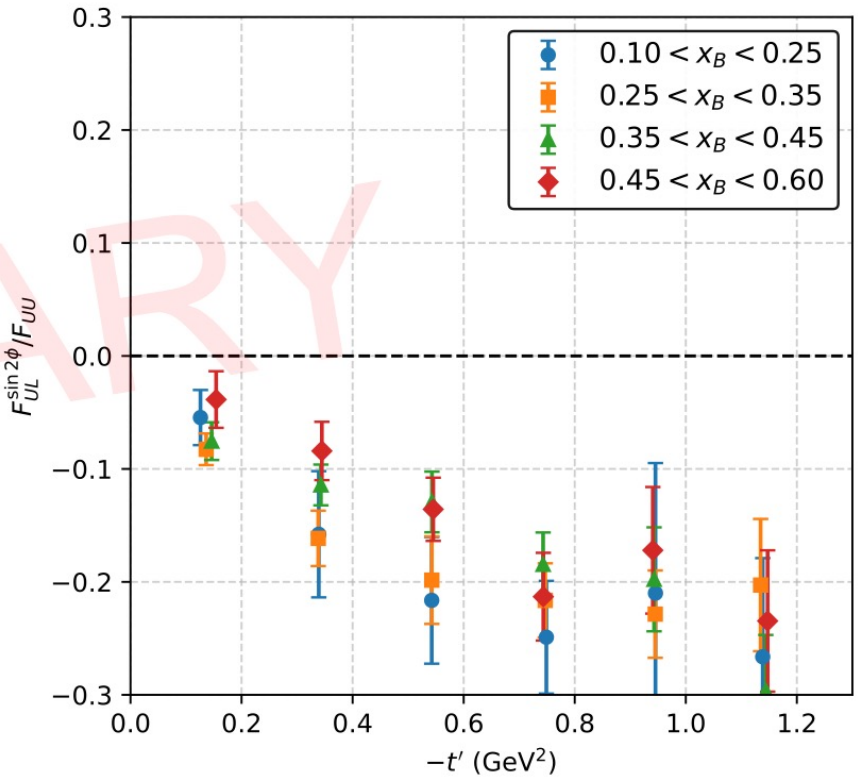

$$A_{UL}^{\sin 2\phi}\,\sigma_0^M = -\,e_0^2(1-\xi^2)\,\eta_M\,\frac{t'}{4m^2}\,\mathrm{Im}\left\{\left[\langle H_T^M\rangle_{TL}^* - \frac{\xi}{1-\xi^2}\,\langle E_T^M\rangle_{TL}^*\right]\langle \tilde{H}_T^M\rangle_{TL}\right\},$$

$$A_{UL}^{\sin 2\phi}\,\sigma_0^M = e_0^2\mathcal{P}^2\mathrm{Im}\left\{\left[\langle H_T^M\rangle_{TL}^* - \frac{\xi}{1-\xi^2}\,\langle E_T^M\rangle_{TL}^*\right]\langle \tilde{H}_T^M\rangle_{TL}\right\},$$

- The sin2ϕ TSA is TT interference, built purely from chiral-odd GPDs (as opposed to the LT asymmetries being generated from interference between chiral-even and chiral-odd GPDs).
- Clear nonzero asymmetry indicates nonzero chiral-odd GPDs. In particular:

$$\tilde{H}_T^M \neq 0$$

$$H_T^M - \frac{\xi}{1-\xi^2}E_T^M \neq 0$$

$$\mathrm{phase}\left(H_T^M - \frac{\xi}{1-\xi^2}E_T^M\right) \neq \mathrm{phase}\left(\tilde{H}_T^M\right)$$

- **First observation!**
- π^+ accesses u-d isovector distribution
- u and d quarks show opposite-signed quadrupole anisotropy in transverse spatial distributions

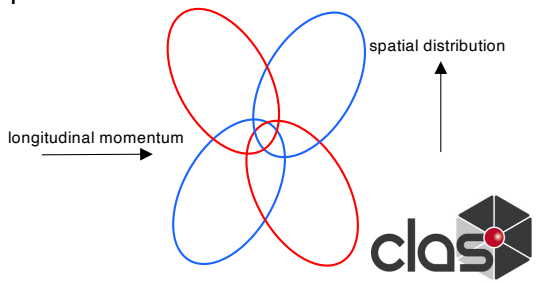

Model Comparisons to RGC Measurement

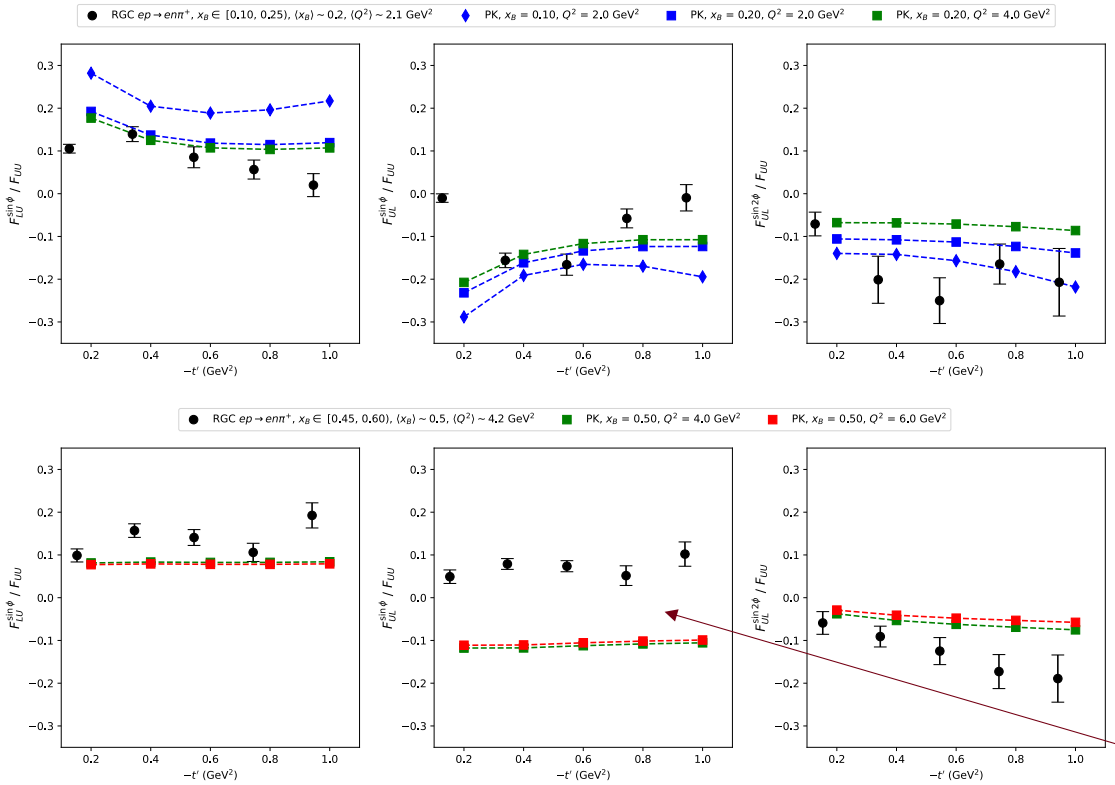

(M. Kerr, MIT)

1. $F_{LU}^{\sin\phi}$ predictions decrease with x_B while data increases with x_B.
2. $F_{UL}^{\sin\phi}$ consistently predicted negative (like HERMES) while sign flip is observed in the data in the valence region.
3. $F_{UL}^{\sin 2\phi}$ always predicted negative and increasing with –t, as in data.

Goloskokov & Kroll, Eur. Phys. J. C **65** (2010) 137; [arXiv:0906.0460]

involves the helicity-flip GPD H_T [17]. As we are going to demonstrate below the data on the spin asymmetry obtained with a transversely polarized target [10] demand this contribution. With respect to the fact that we need three (almost) unknown GPDs for exclusive π^+ electroproduction we consider our analysis as a rather qualitative study, not all aspects of the data will be accommodated well. Yet we think of our work as the next step towards a comprehensive analysis of hard exclusive meson electroproduction.

Fermi Motion

- Nuclei inside of the nucleus are not at rest but instead occupy quantum states up to the Fermi momentum.
- Typical scales of around 100-200 MeV or higher depending on the nuclei (heavier nuclei = more momentum).
- In lepton scattering our physics observables depend on kinematics defined by the initial and final state particles. For RGA-like experiments the target can be safely be considered at rest but not in nuclear experiments.
- When we incorrectly use p = 0 for the target nucleon we calculate the incorrect final kinematics and interpret this as “Fermi smearing” (caused by Fermi Motion).
- This causes, for example, the resolution of missing mass peaks to be much worse in carbon compared to liquid hydrogen.

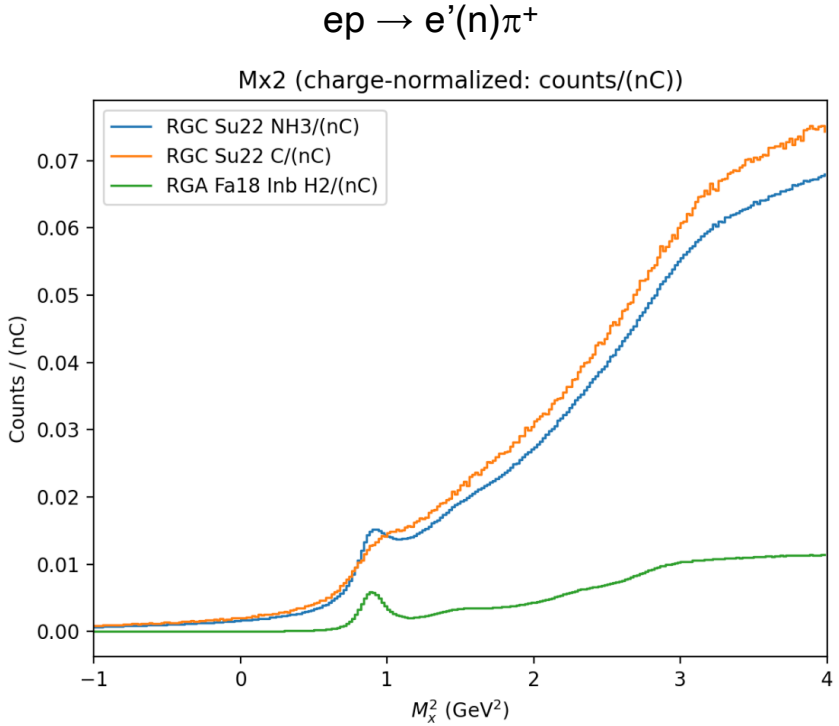

Simulating Fermi Motion

- Starting from the tabulated n(k) distributions a corresponding probability density was constructed so that the CDF is

$$N(k_j) = \int_0^{k_j} F(k)dk$$

with normalization $N(k_{max}) = 1$.

- For each event a random number $r \in [0,1]$ is chosen and the CDF inverted to obtain a momentum magnitude k such that N(k) = r.
- Convert to conventional units by multiplying by $\hbar c \sim 0.1973$ GeV fm.
- Finally, an isotropic distribution is generated by drawing ϕ and θ uniformly on a sphere and forming the unit vector

$$\hat{p} = (\sin\theta\cos\phi,\ \sin\theta\sin\phi,\ \cos\theta)$$

such that the simulated Fermi motion is $\vec{p}_F = p\hat{p}$.

AV18 (high precision two-body fit to NN data)/**UIX** (three-body forces with correct binding energy and structures) Hamiltonian, is solved via variational Monte Carlo integration using stochastic sampling to provide nucleon momentum n(k) as momentum-space probability densities:

k[fm-1]	D2	He4	Be8	C12	N14	O16
0.000000	13.021000	0.880840	0.517839	0.154807	0.163119	0.171430
0.100000	9.100200	0.844150	0.511187	0.178190	0.183235	0.188280
0.200000	4.062200	0.744980	0.488208	0.231405	0.225102	0.218800
0.300000	1.633000	0.611140	0.445071	0.278976	0.262783	0.246590
0.400000	0.684670	0.471660	0.383793	0.295908	0.276924	0.257940
0.500000	0.308920	0.346490	0.312840	0.279177	0.263379	0.247580
0.600000	0.149450	0.245100	0.241685	0.238258	0.228534	0.218810
0.700000	0.076714	0.168270	0.177847	0.187422	0.183451	0.179480
0.800000	0.041375	0.112800	0.125277	0.137754	0.137812	0.137870
0.900000	0.023276	0.074095	0.084963	0.095827	0.097877	0.099926
1.000000	0.013592	0.047851	0.055815	0.063777	0.066275	0.068773
1.100000	0.008216	0.030473	0.035719	0.040963	0.043066	0.045168
1.200000	0.005135	0.019193	0.022375	0.025555	0.026994	0.028433
1.300000	0.003320	0.012017	0.013836	0.015654	0.016454	0.017254
1.400000	0.002221	0.007535	0.008520	0.009506	0.009841	0.010175
1.500000	0.001540	0.004777	0.005301	0.005825	0.005874	0.005923
1.600000	0.001107	0.003113	0.003392	0.003672	0.003586	0.003499
1.700000	0.000823	0.002117	0.002276	0.002435	0.002312	0.002190
1.800000	0.000632	0.001524	0.001625	0.001727	0.001622	0.001516
1.900000	0.000499	0.001168	0.001241	0.001315	0.001247	0.001180

R.B. Wiringa, VMC results using the AV18/UIX Hamiltonian (Argonne v18 + Urbana IX). Numerical results obtained from Variational Monte Carlo (VMC) calculations with the AV18/UIX Hamiltonian; provided via A. El Alaoui in private correspondence.

Smearing Results on RGA

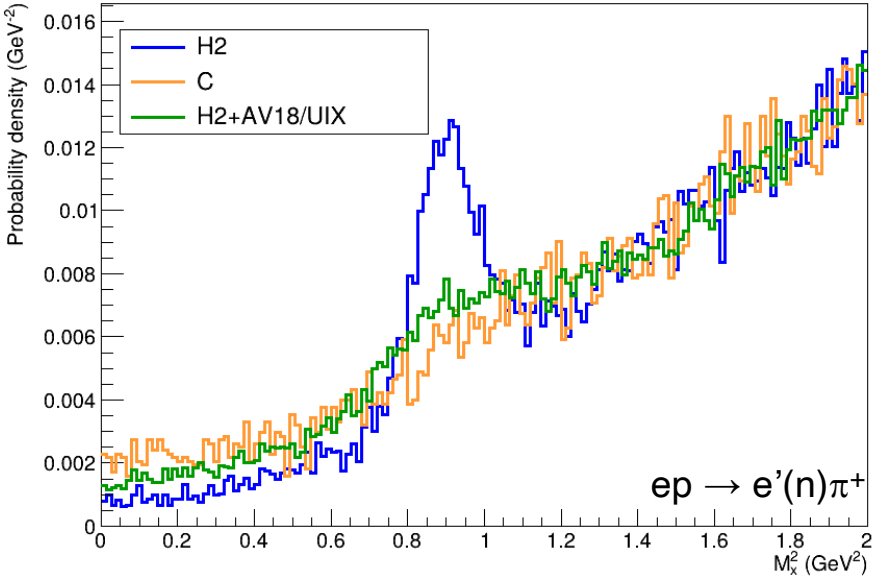

- RGA can be used to validate the smearing effects by comparing missing mass distributions reconstructed with the target assumed to be at rest and with the target assigned a momentum randomly chosen via the previously described method.

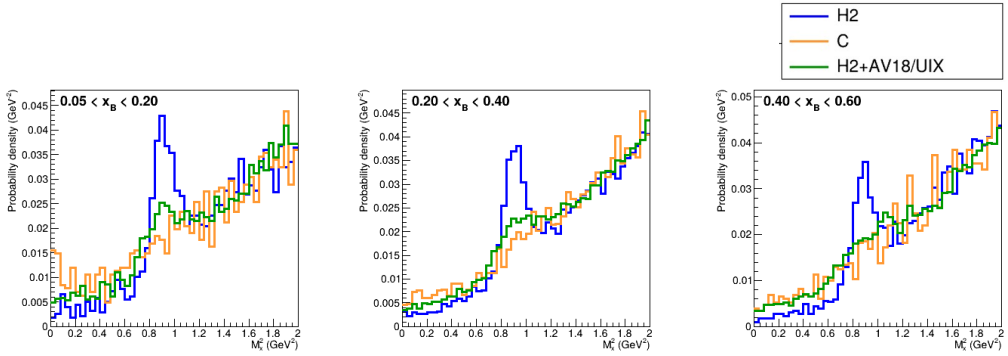

Migration Effects

- “Migration” can come from many different sources: detector resolution effects, radiative effects, motion in the nuclear medium, etc.
- Detector resolution effects come from imprecise measurements (we use the “incorrect” final state kinematics, e.g. pion polar angle).
- Radiative effects come from us using the wrong kinematics to reconstruct our event, whether that is before or after interaction with the virtual photon (e.g. incoming or outgoing electron momentum).
- Nuclear (“Fermi”) motion comes from using the wrong four-vector for the initial target nucleon. We never measure the target and so incorrectly assume the nucleon to be at rest. This is a good assumption for the hydrogen target experiments but is incorrect for the nuclear targets.
- We bin our asymmetries in x_B and t. Fermi motion does not *strongly* affect our reconstruction of these variables, *but* it can pull down events which are more properly in the higher missing mass/non-exclusive region into our data sample. This is critical because the physics is very different in that region.

Fermi motion shifts:

Observable	Δ(observable) from assuming $p = (M, 0)$
$x_B = \dfrac{Q^2}{2p \cdot q}$	$\Delta x_B = \dfrac{Q^2}{2M\nu} - \dfrac{Q^2}{2(M\nu - \vec{p}_F \cdot \vec{q})} \approx x_B \dfrac{\vec{p}_F \cdot \vec{q}}{M\nu}$
$t = (q - p_\pi)^2$	$\Delta t = (p_p - p^{(0)})^2 - (p_p - p)^2 \approx 2\,\vec{p}_F \cdot \vec{p}_p$
$M_x^2 = (q + p - p_\pi)^2$	$\Delta M_x^2 = (q + M - p_\pi)^2 - (q + p - p_\pi)^2 \approx -2\,\vec{p}_F \cdot (\vec{q} - \vec{p}_\pi)$

Rough **Fermi Motion Size Estimates from Data**

- Taking advantage of the en → e'pπ^- final state where you measure all final state particle (note: that is not *all* particles!).
- Assumptions/reason for roughness: exclusivity ($M_x^2 < 1.07$ GeV^2; ~80% truth c.f. next slides) and perfect precision.
- Calculate difference in kinematics assuming at rest neutron and calculated neutron momentum.

RGB

RGC ND_3

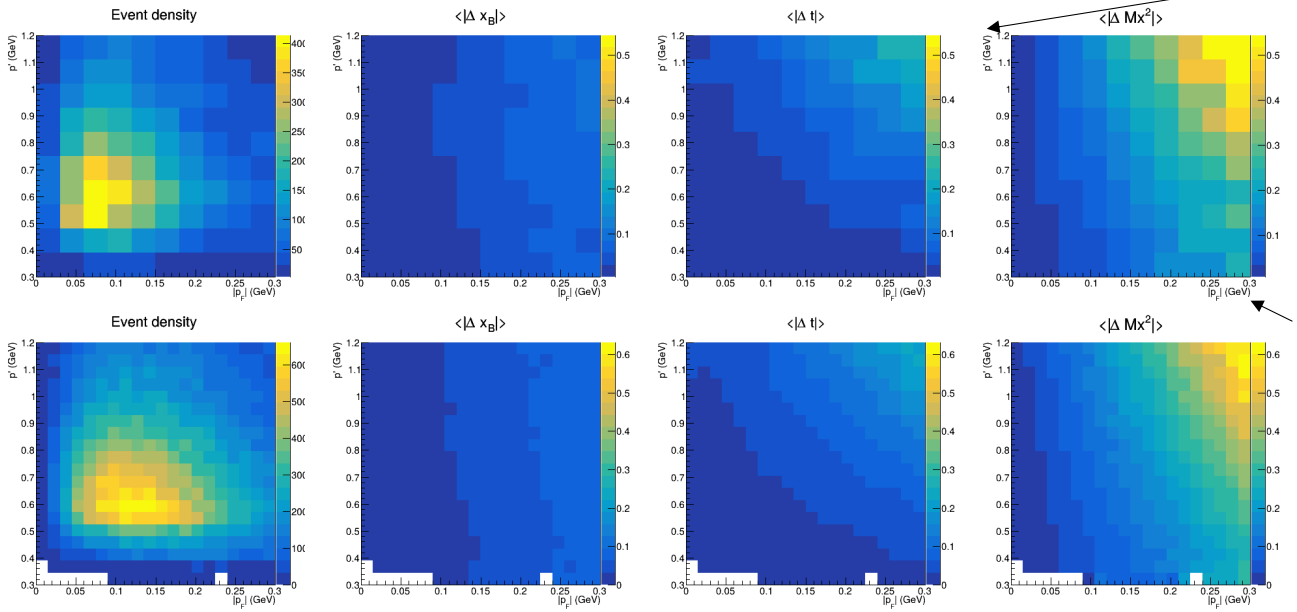

Creation of MC

- clasdis does contain “exclusive” enπ^+ events but they do not exist at the lowest x_B values.
- A dedicated exclusive meson generator, aaogen, was used to simulate exclusive π^+ events and mix them with clasdis to reproduce the measured eπ^+X background.
- clasdis built from sample with 10/7 proton/neutron target and then combined with aaogen from proton target.
- Both generators were mixed according to

$$H_{\mathrm{mix}}(M_x^2) = wH_{\mathrm{aaogen}}(M_x^2) + (1-w)H_{\mathrm{clasdis}}(M_x^2)$$

with w chosen to minimize the bin-to-bin discrepancy between H_{mix} and the data.

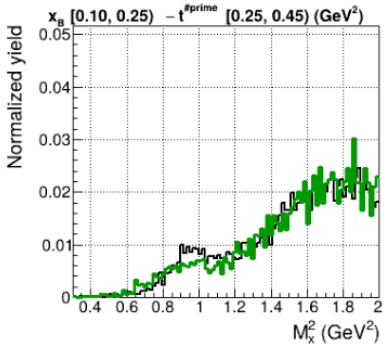

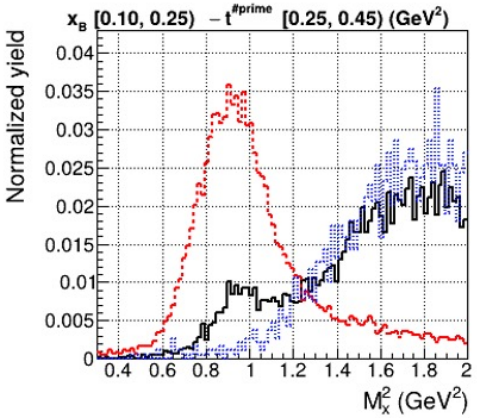

aaogen
clasdis
data

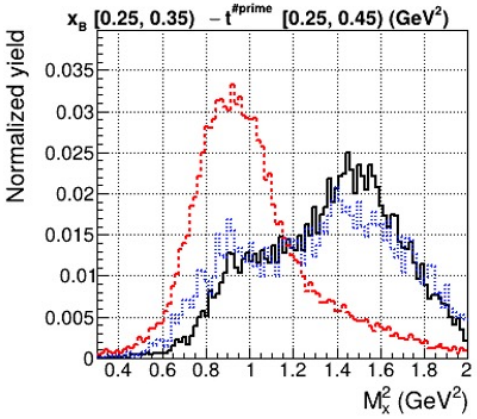

M_x^2 smearing due to Fermi Motion in enπ^+

- Contributions from adjacent missing mass regions can be several percent or higher.
- Size of shift depends on contamination and on the difference between asymmetry values in both regions.
- Single-spin asymmetries ~ 1-2% systematic; double-spin asymmetries ~ 3-5%.

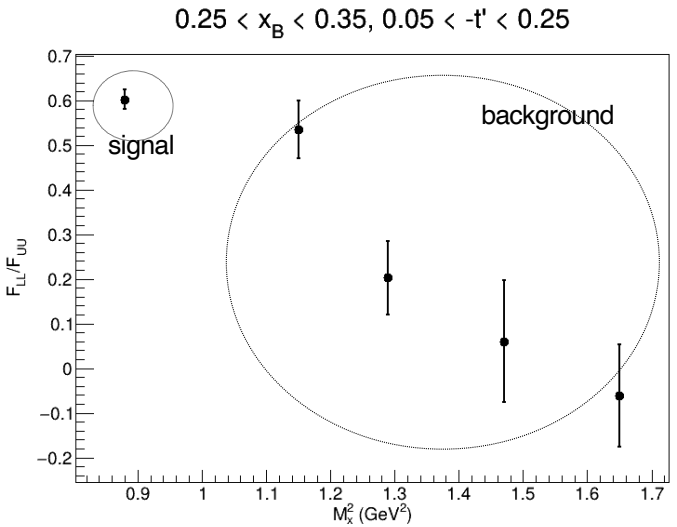

Reconstructed Bin	M_x^2 Range (GeV^2)	Generated Bin					
		0	1	2	3	4	5
0	< 1.07	0.78	0.10	0.04	0.02	0.02	0.04
1	$1.07 - 1.22$	0.62	0.12	0.07	0.05	0.05	0.10
2	$1.22 - 1.37$	0.41	0.10	0.10	0.09	0.10	0.18
3	$1.37 - 1.52$	0.25	0.08	0.11	0.12	0.16	0.27
4	$1.52 - 1.77$	0.14	0.06	0.09	0.11	0.19	0.40
5	> 1.77	0.02	0.01	0.01	0.01	0.03	0.92

Table 10: MC bin-migration matrix for M_x^2 bins. Entries are given as the fractional value of events reconstructed in row i that were generated in column j.

x_B range	$F_{LU}^{\sin\phi}/F_{UU}$	$F_{UL}^{\sin\phi}/F_{UU}$	$F_{UL}^{\sin 2\phi}/F_{UU}$	F_{LL}/F_{UU}	$F_{LL}^{\cos\phi}/F_{UU}$
$0.10 < x_B < 0.25$	[0.004, 0.007, 0.010]	[0.002, 0.014, 0.026]	[0.005, 0.021, 0.053]	[0.008, 0.029, 0.059]	[0.011, 0.033, 0.068]
$0.25 < x_B < 0.35$	[0.000, 0.009, 0.020]	[0.004, 0.007, 0.013]	[0.004, 0.023, 0.056]	[0.001, 0.020, 0.036]	[0.001, 0.042, 0.156]
$0.35 < x_B < 0.45$	[0.001, 0.009, 0.021]	[0.000, 0.004, 0.013]	[0.013, 0.023, 0.044]	[0.009, 0.031, 0.066]	[0.005, 0.028, 0.054]
$0.45 < x_B < 0.60$	[0.003, 0.011, 0.020]	[0.001, 0.005, 0.010]	[0.005, 0.024, 0.043]	[0.005, 0.032, 0.050]	[0.003, 0.034, 0.073]

Table 12: Bin-migration shift due to Fermi motion. For each x_B range: [min|Δ|, ⟨|Δ|⟩, max|Δ|] across available $-t'$ points for each polarized structure-function ratio.

Effects from Initial and Final State Radiation

- Radiative photons modify the reconstructed virtual photons 4-momentum.
- FSR effects are reduced compared to ISR (lower energy lepton); accounted for to first order by adding the 4-vectors of photons in a cone angle around the scattered electron when reconstructing k'.
- ISR is simulated with an iterative procedure using a photon energy distribution generated from RADGEN.

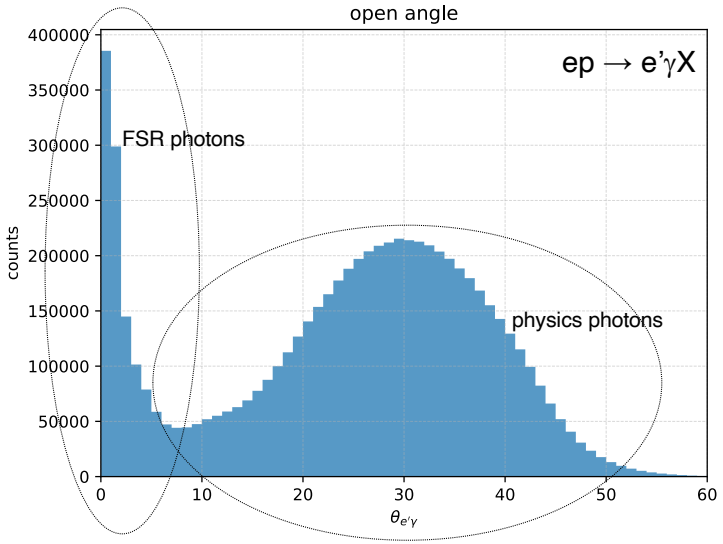

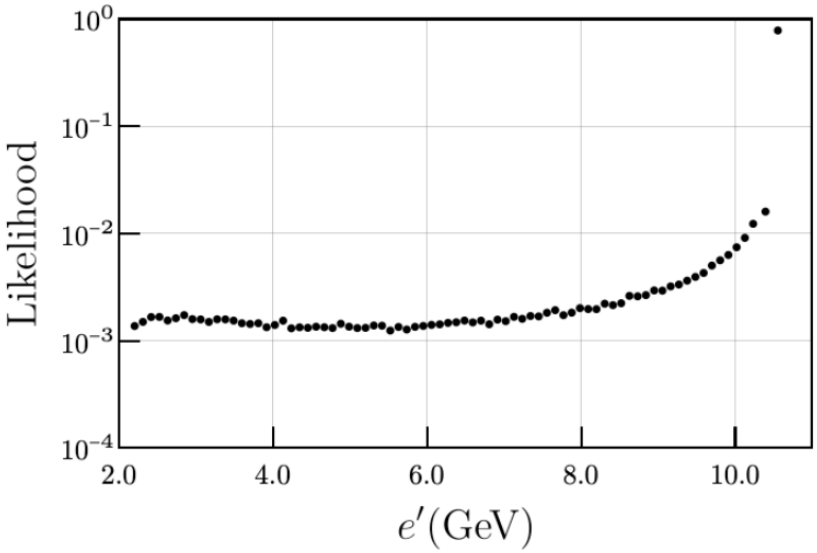

Estimating ISR

Δ_{rad} = true physics radiation
Δ_{rad}' = simulated RADGEN radiation

$$A_{\text{baseline}} = A_{\text{Born}} + \Delta_{\text{rad}},$$
$$A_{\text{sim. ISR/FSR}} = A_{\text{Born}} + \Delta_{\text{rad}} + \Delta_{\text{rad'}},$$
$$\Delta_{\text{rad}} \approx \Delta_{\text{rad'}}$$
$$A_{\text{sim. ISR/FSR}} = A_{\text{Born}} + 2\Delta_{\text{rad}}$$

simulated additional RADGEN radiation on an event-by-event basis

$$\Delta_{\text{rad}} = A_{\text{sim. ISR/FSR}} - A_{\text{baseline}},$$
$$A_{\text{Born}} = A_{\text{baseline}} - \left(A_{\text{sim. ISR/FSR}} - A_{\text{baseline}}\right),$$
$$A_{\text{Born}} = 2A_{\text{baseline}} - A_{\text{sim. ISR/FSR}},$$

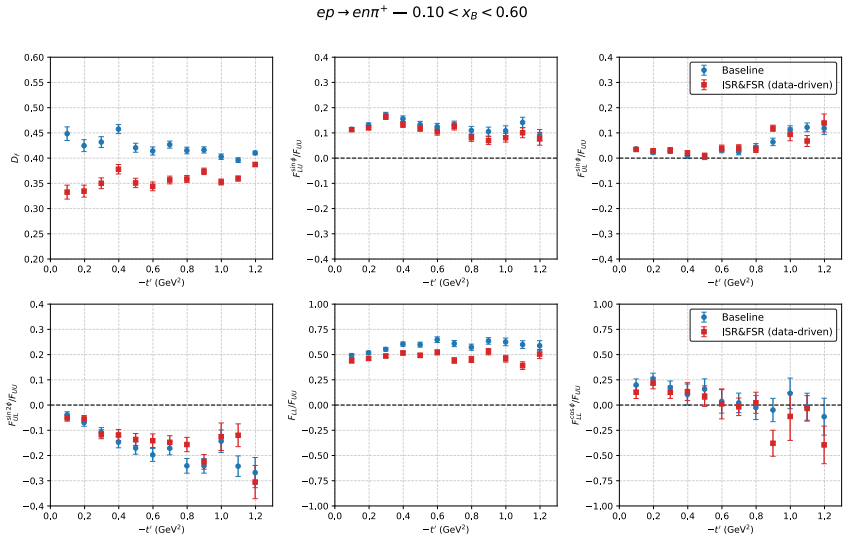

measured asymmetries
measured asymmetries + additional RADGEN

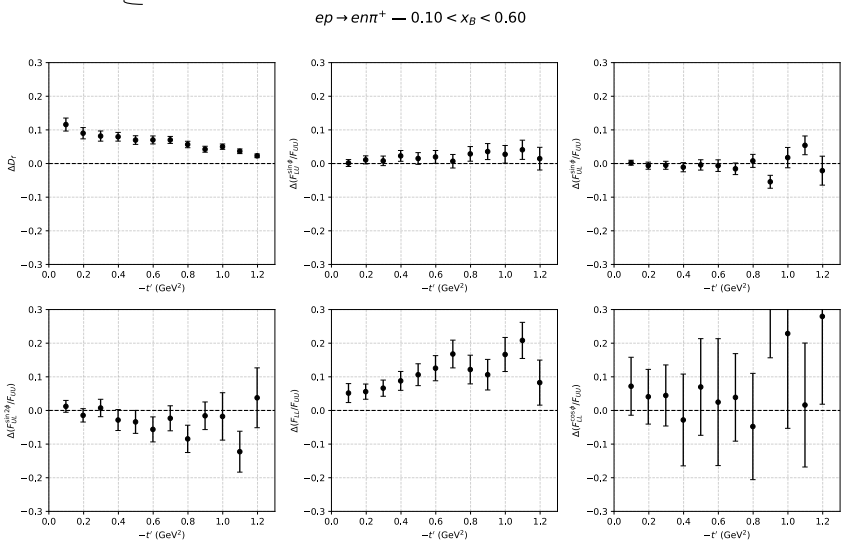

size of radiative correction

Conclusions

- RGC has been rigorously studied for stability across different run periods and configuration changes.
- Systematics from radiation, nuclear motion, detector resolution, tangentially polarized target contributions, particle identification, etc. have been evaluated.
- The analysis of exclusive π^+ production off NH_3 is tentatively complete and has entered working group review:
  1. Observation of negative $A_{UL}\sin\phi$ for low x_B by HERMES is confirmed.
  2. First observation of nonzero $A_{UL}\sin2\phi$ is observed (TT interference: chiral-odd GPDs, in particular $\tilde{H}_T^M$ confirmed nonzero!).
  3. Rich structure function extraction (5+ modulations) and comparison with predictions of GK model predictions allow for deep phenomenological study. Constraints with theory predictions set the scale for the contributions of often previously ignored chiral-odd GPDs.
  4. Aiming for publication in PRL.

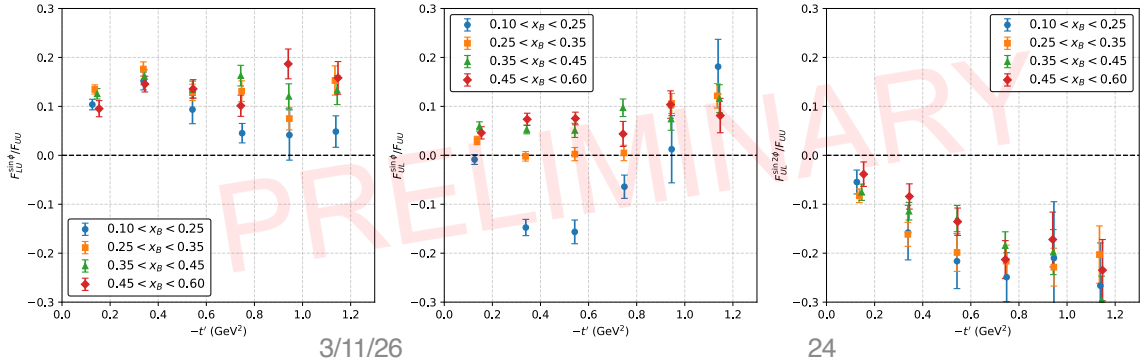

Results

- All five accessible polarized structure functions are measured for the ep → e'π^+(n) channel in 24 multidimensional bins in x_B and –t'.

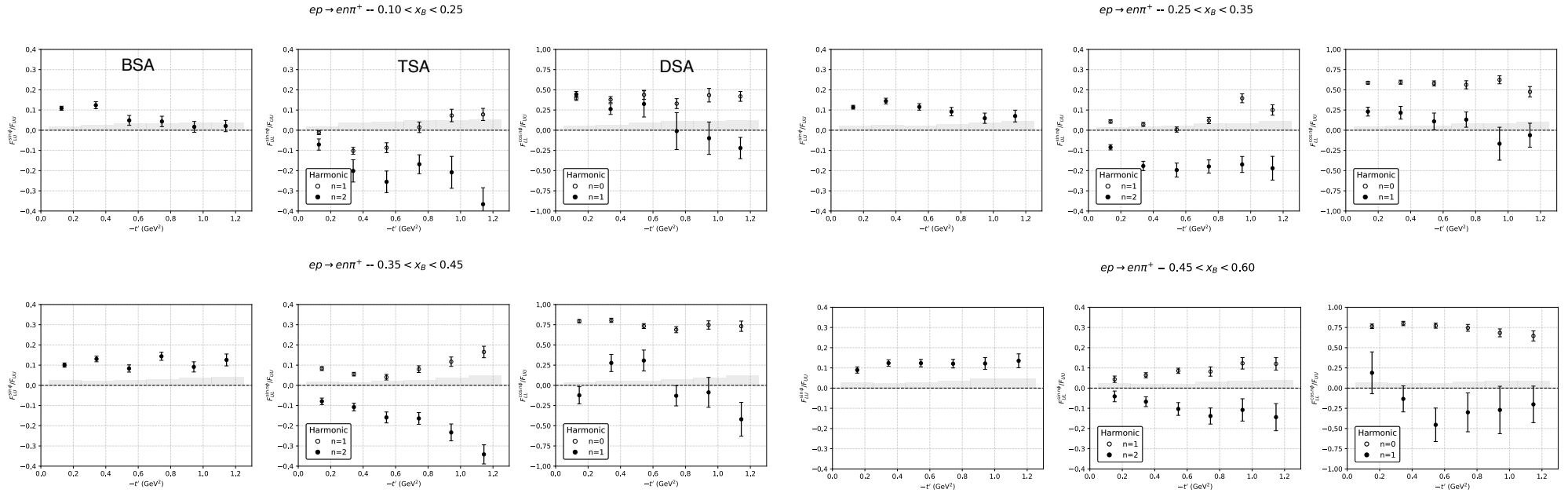

Back up

HERMES TSA measurements

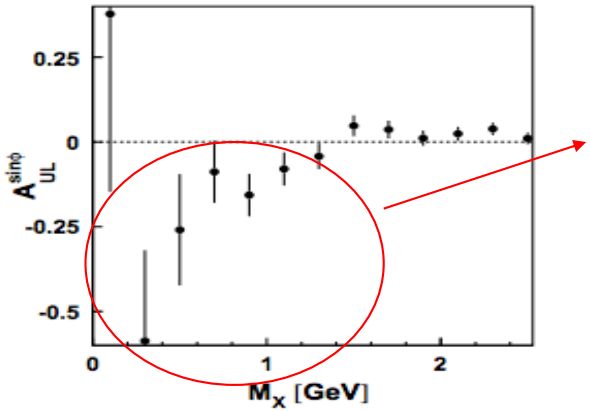

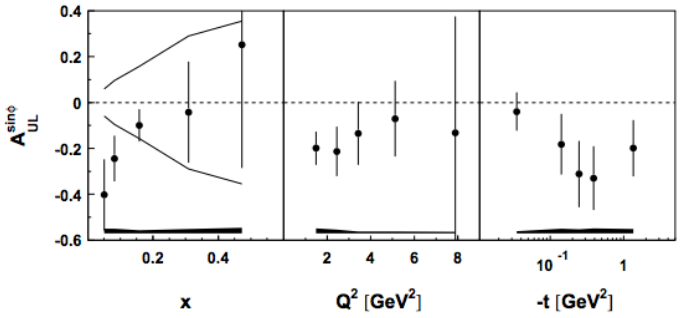

Phys.Lett.B 535 (2002) 85-92 [hep-ex/0112022]

- The low statistics measurement from HERMES shows a large negative asymmetry in the exclusive region.
- CLAS(12) BSA measurements had shown positive asymmetry.
- Traditionally BSA ~ TSA.

- Similarly, measurements for exclusive π^+ and π^- were shown to have the same sign.

$$ep \rightarrow e'\pi^+ n$$

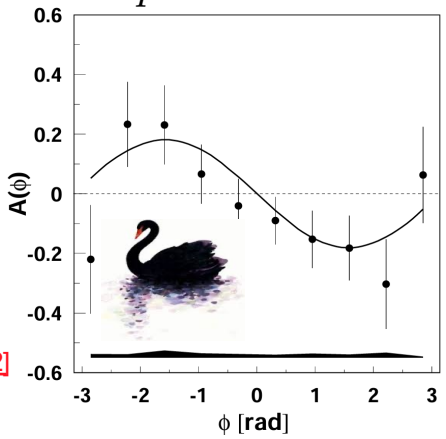

Phys.Lett.B 562 (2003) 182-192 [hep-ex/0212039]

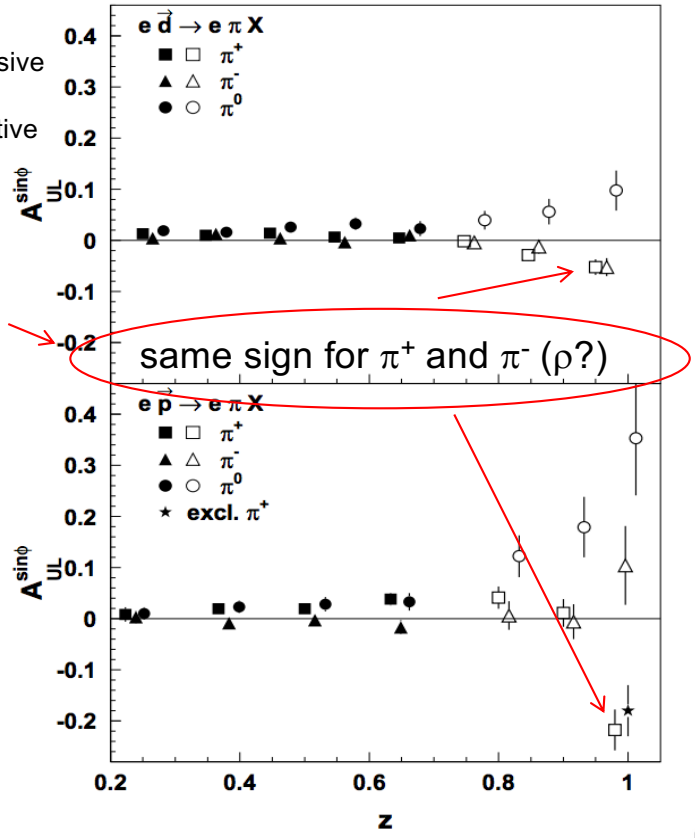

Kinematic Distributions

Binning scheme:

x_B [0.10,0.25,0.35,0.45,0.60]

-t [0.05,0.15,0.25,0.35,0.45,0.55, 0.65,0.75,0.85, 0.95,1.05,1.15,1.25]

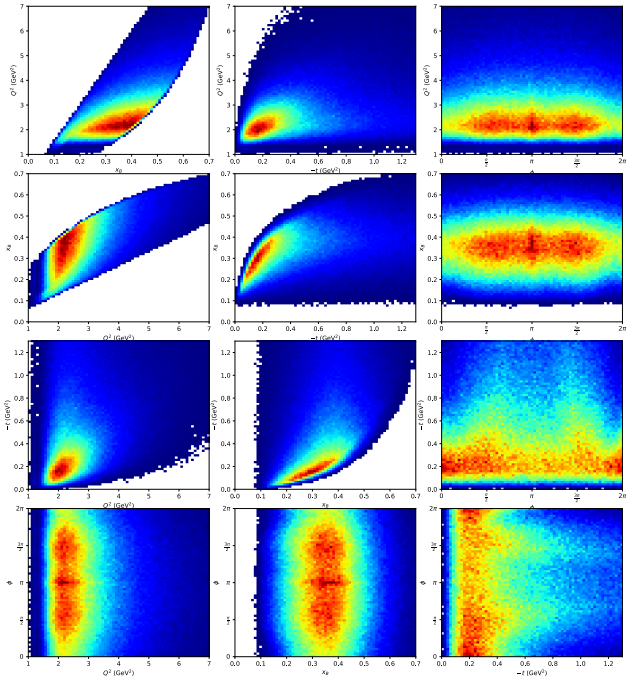

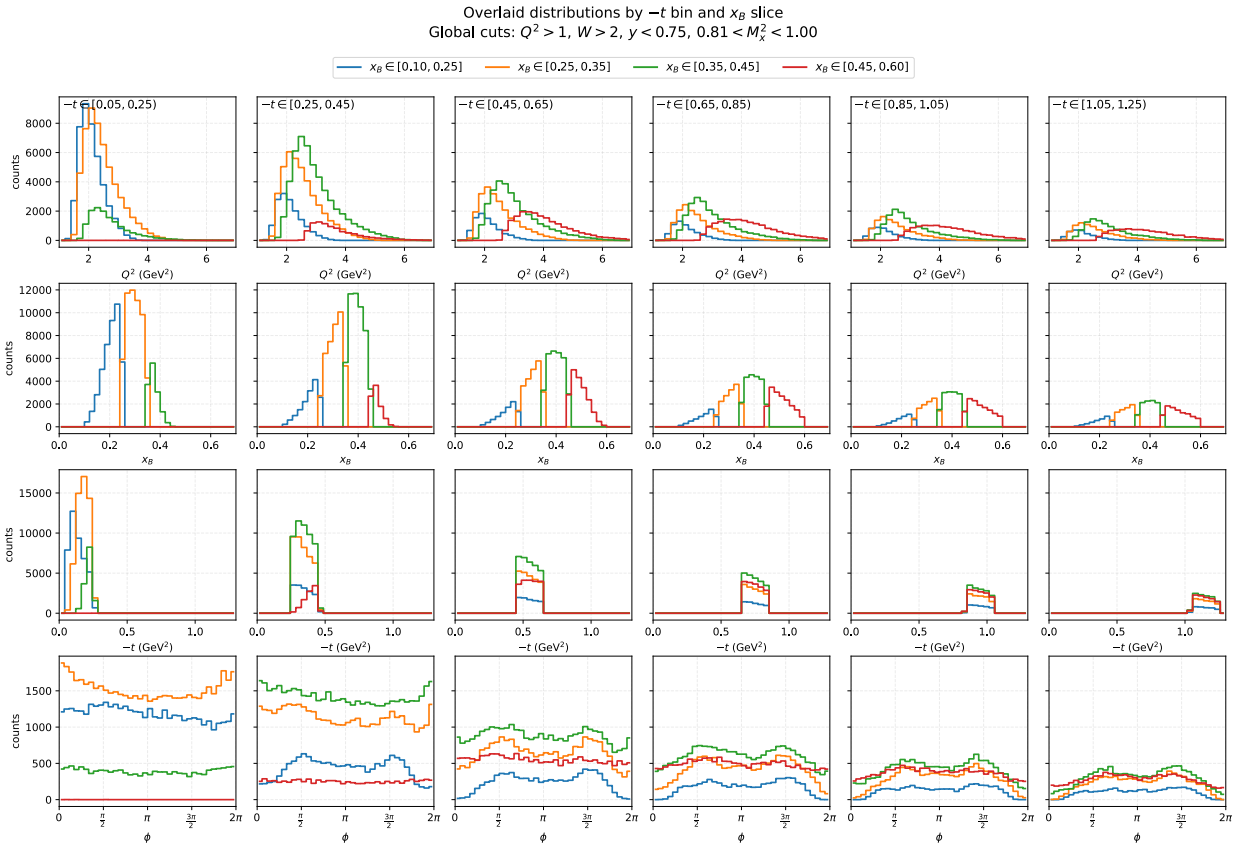

Dilution Factors

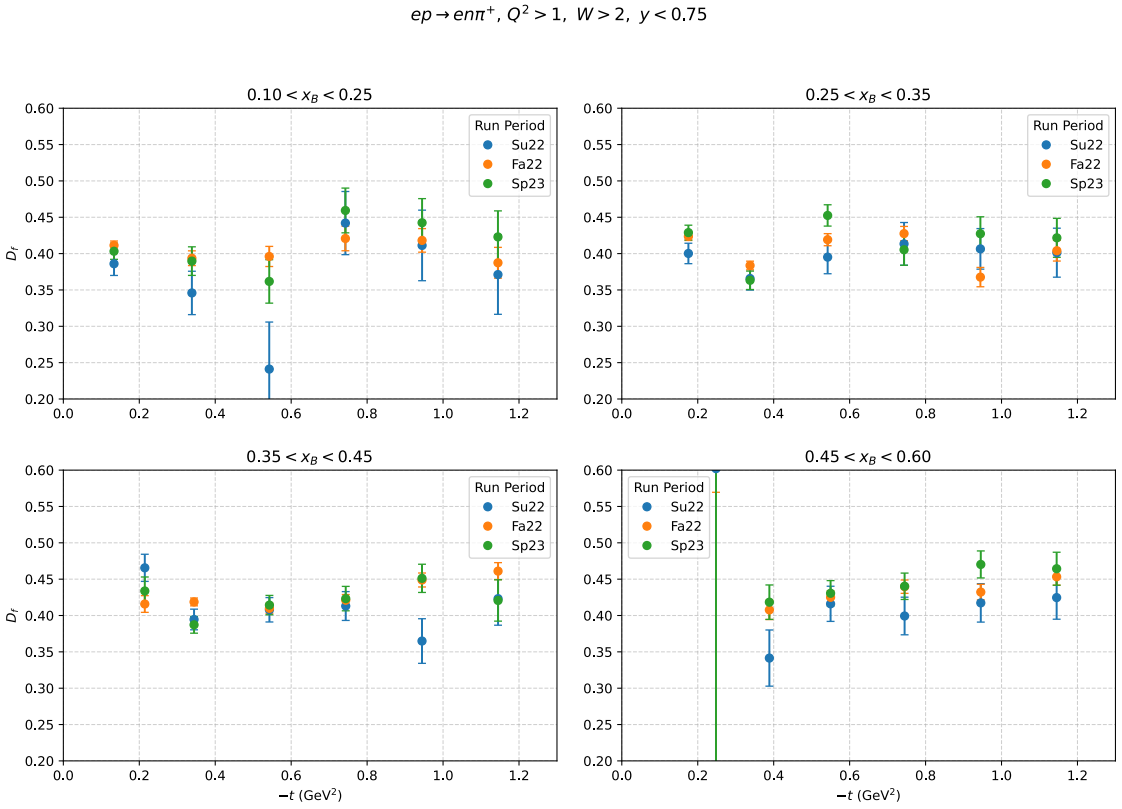

- Dilution factor extracted independently in each bin and for each run period.
- Minimal kinematic dependence in x_B or –t.
- Dilution factor approximately 40%.

Run Period Stability

- Asymmetry extraction is performed independently for each run period and then combined. Statistical tests (χ^2 and p-test) indicate consistency between all three periods.

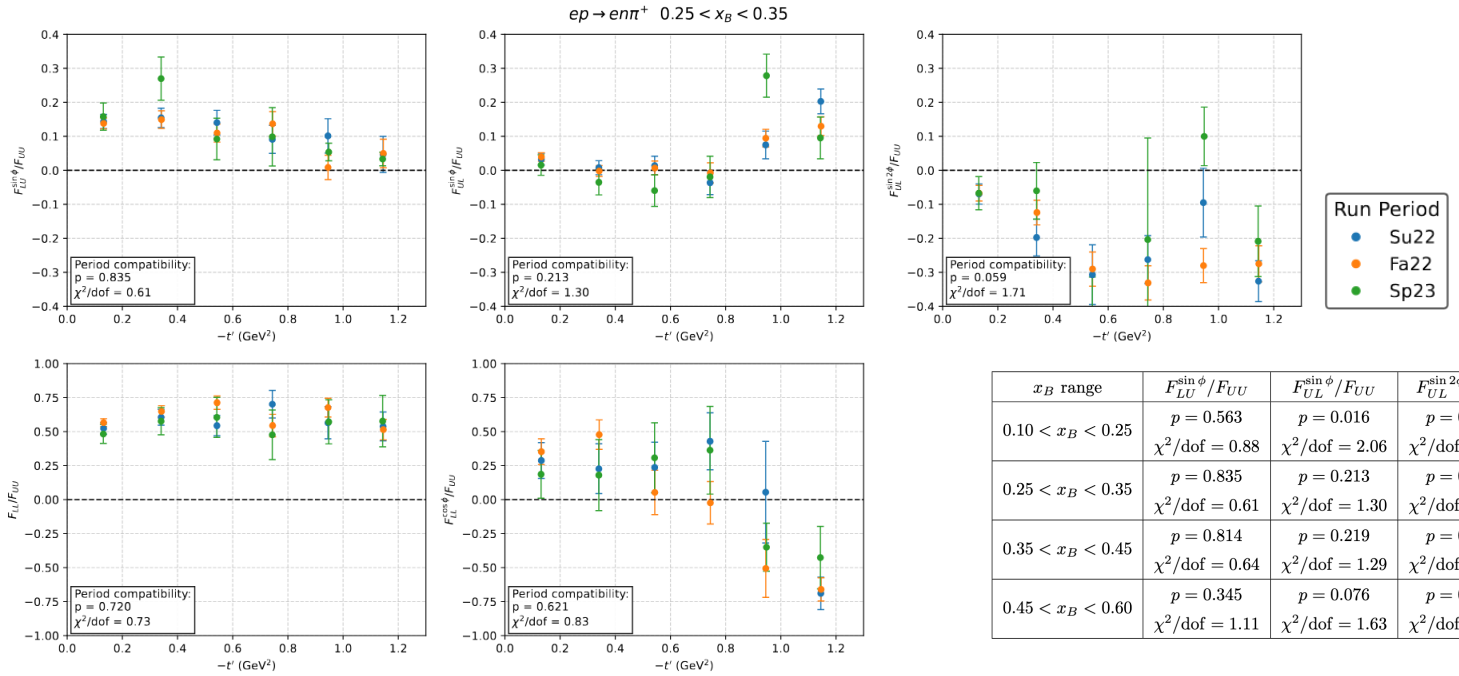

x_B range	$F_{LU}^{\sin\phi}/F_{UU}$	$F_{UL}^{\sin\phi}/F_{UU}$	$F_{UL}^{\sin 2\phi}/F_{UU}$	F_{LL}/F_{UU}	$F_{LL}^{\cos\phi}/F_{UU}$
$0.10 < x_B < 0.25$	$p = 0.563$ $\chi^2/\text{dof} = 0.88$	$p = 0.016$ $\chi^2/\text{dof} = 2.06$	$p = 0.047$ $\chi^2/\text{dof} = 1.77$	$p = 0.137$ $\chi^2/\text{dof} = 1.44$	$p = 0.078$ $\chi^2/\text{dof} = 1.62$
$0.25 < x_B < 0.35$	$p = 0.835$ $\chi^2/\text{dof} = 0.61$	$p = 0.213$ $\chi^2/\text{dof} = 1.30$	$p = 0.059$ $\chi^2/\text{dof} = 1.71$	$p = 0.720$ $\chi^2/\text{dof} = 0.73$	$p = 0.621$ $\chi^2/\text{dof} = 0.83$
$0.35 < x_B < 0.45$	$p = 0.814$ $\chi^2/\text{dof} = 0.64$	$p = 0.219$ $\chi^2/\text{dof} = 1.29$	$p = 0.604$ $\chi^2/\text{dof} = 0.84$	$p = 0.695$ $\chi^2/\text{dof} = 0.76$	$p = 0.547$ $\chi^2/\text{dof} = 0.90$
$0.45 < x_B < 0.60$	$p = 0.345$ $\chi^2/\text{dof} = 1.11$	$p = 0.076$ $\chi^2/\text{dof} = 1.63$	$p = 0.214$ $\chi^2/\text{dof} = 1.29$	$p = 0.128$ $\chi^2/\text{dof} = 1.47$	$p = 0.006$ $\chi^2/\text{dof} = 2.32$

Comparisons to RGA

- The RGA H_2 distribution can be suitably reconstructed from RGC data by removing the nuclear background from the ammonia target.

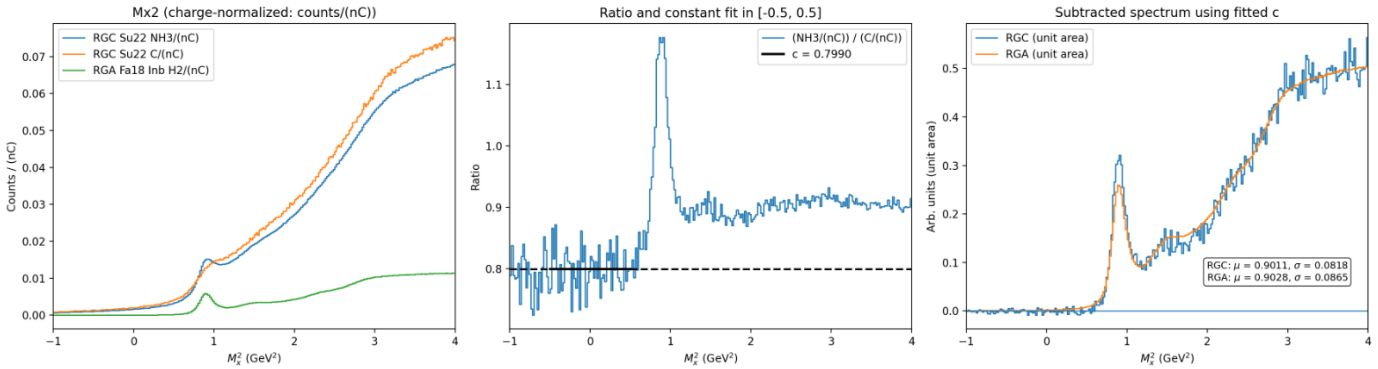

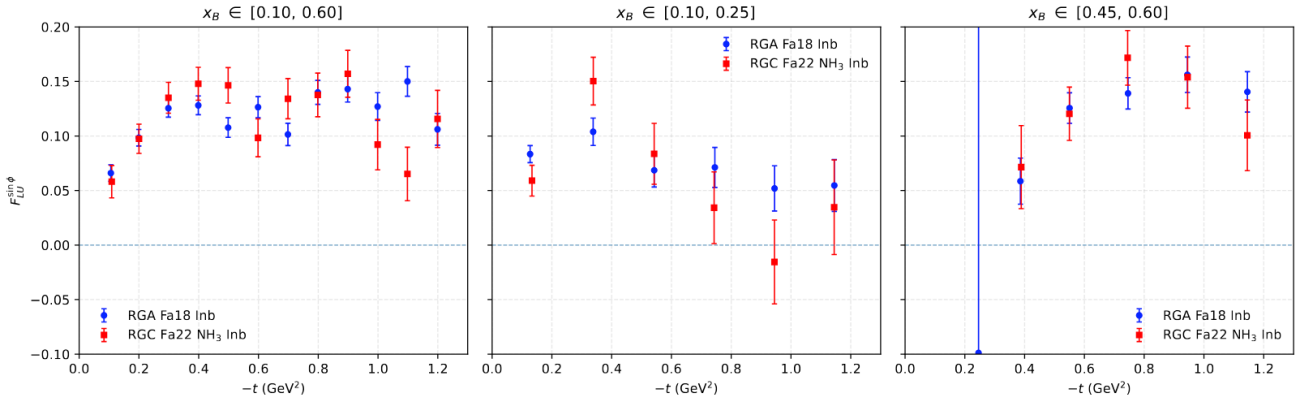

- RGA and RGC exclusive π^+ asymmetries are consistent.
- No strong nuclear effect observed within the precision of our measurement.

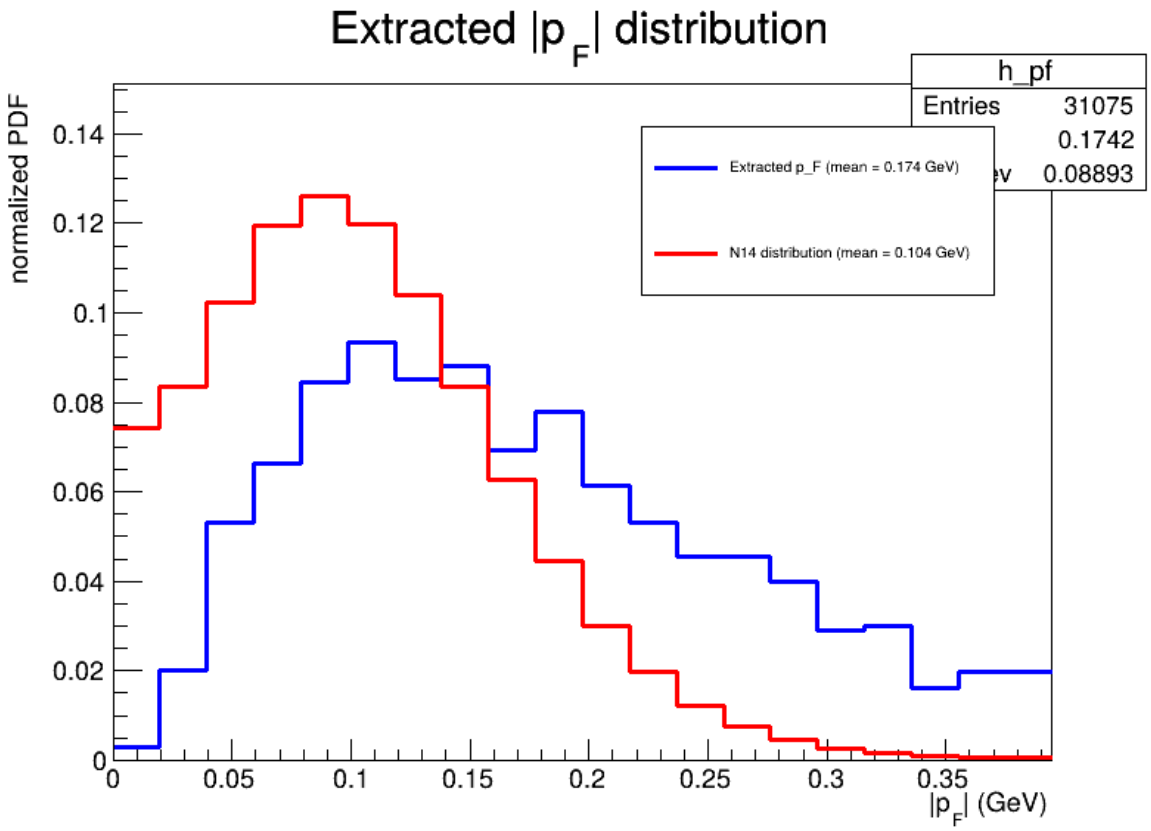
Extracted |p_F| distribution
h_pf
Entries 31075
0.1742
0.08893
Extracted p_F (mean = 0.174 GeV)
N14 distribution (mean = 0.104 GeV)
normalized PDF
0.14
0.12
0.1
0.08
0.06
0.04
0.02
0
0
0.05
0.1
0.15
0.2
0.25
0.3
0.35
|p_F| (GeV)

Comparison between BSA and TSA

Goloskokov & Kroll, Eur. Phys. J. C **65** (2010) 137; [arXiv:0906.0460]

$$A_{LU}^{\sin\phi}\,\sigma_0^M = e_0^2\sqrt{1-\xi^2}\,\frac{\sqrt{-t'}}{2m}\,\mathrm{Im}\Big\{2\,\langle E_T^M\rangle_{TL}^*\,\langle H_{\rm eff}^M\rangle_{LL} + \Big[-2\,\langle H_T^M\rangle_{TL}^* + \frac{2\xi}{1-\xi^2}\,\langle E_T^M\rangle_{TL}^*\Big]\,\langle E^M\rangle_{LL}\Big\}, \tag{3}$$

$$A_{UL}^{\sin\phi}\,\sigma_0^M = e_0^2\sqrt{1-\xi^2}\,\frac{\sqrt{-t'}}{2m}\,\mathrm{Im}\Big\{2\,\langle \overline{E}_T^M\rangle_{TL}^*\,\langle H_{\rm eff}^M\rangle_{LL} + \Big[\frac{t'}{m^2}\,\langle \tilde{H}_T^M\rangle_{TL}^* - 2\,\langle H_T^M\rangle_{TL}^* + \frac{2\xi}{1-\xi^2}\,\langle E_T^M\rangle_{TL}^*\Big]\,\langle E^M\rangle_{LL}\Big\}. \tag{4}$$

It is convenient to define the overall prefactor

$$\mathcal{P} = \sqrt{1-\xi^2}\,\frac{\sqrt{-t'}}{2m}, \tag{5}$$

and express the observables as

$$A_{LU}^{\sin\phi}\,\sigma_0^M = e_0^2\mathcal{P}\,(\mathcal{C}+\mathcal{D}_{LU}), \qquad A_{UL}^{\sin\phi}\,\sigma_0^M = e_0^2\mathcal{P}\,(\mathcal{C}+\mathcal{D}_{UL}), \tag{6}$$

where the common contribution is

$$\mathcal{C} = \mathrm{Im}\Big\{\Big[-2\,\langle H_T^M\rangle_{TL}^* + \frac{2\xi}{1-\xi^2}\,\langle E_T^M\rangle_{TL}^*\Big]\,\langle E^M\rangle_{LL}\Big\}, \tag{7}$$

and the distinct pieces are

$$\mathcal{D}_{LU} = \mathrm{Im}\Big\{2\,\langle E_T^M\rangle_{TL}^*\,\langle H_{\rm eff}^M\rangle_{LL}\Big\}, \tag{8}$$

$$\mathcal{D}_{UL} = \mathrm{Im}\Big\{2\,\langle \overline{E}_T^M\rangle_{TL}^*\,\langle H_{\rm eff}^M\rangle_{LL} + \frac{t'}{m^2}\,\langle \tilde{H}_T^M\rangle_{TL}^*\,\langle E^M\rangle_{LL}\Big\}. \tag{9}$$

reminder: $\bar{E} = 2\tilde{H}_T + E_T$

- GK model predict negative A_{UL}; we mostly measure positive values with $A_{UL} \sim A_{LU}$.
- Either the GK model underpredicts the C term or over predicts the D_{UL} term. The fact that $A_{LU} \sim A_{UL}$ would seem to indicate the C term dominates.
- Because the $A_{UL}\sin2\phi$ is predicted well (which contain H_T, E_T and $\tilde{H}_T$), the logical conclusion is that E_{LL}^M is being underestimated.

$$\begin{aligned} c_{1,\mathrm{TP}-}^{\mathrm{I}} \;\propto\; & -\frac{M}{Q}\,\mathrm{Im}\Big\{\frac{t}{4M^2}\Big[(2-x_B)F_1\mathcal{E} - 4\frac{1-x_B}{2-x_B}F_2\mathcal{H}\Big] \\ & + \; x_B\xi\Big[F_1(\mathcal{H}+\mathcal{E}) - (F_1+F_2)(\tilde{\mathcal{H}}+\frac{t}{4M^2}\tilde{\mathcal{E}})\Big]\Big\}, \end{aligned} \tag{11}$$

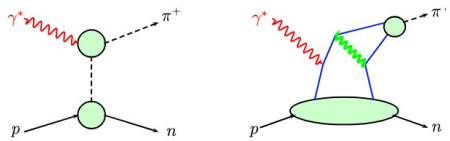

Figure 1: The pion pole (left) and the handbag (right) contribution to electroproduction of positively charged pions.

The pion pole contribution, see Fig. 1, with the residue ρ_π and pion mass m_π, will be discussed in the next section in some detail. In constrast to other work [12, 13, 14, 15] but in view of the fact that we take into account the full pion form factor and not just its perturbative contribution, we write the pion pole contributions and those from $\tilde{E}^{(3)}$ separately, i.e. our $\tilde{E}^{(3)}$ only represents the non-pole contribution of the full GPD. For large Q^2, $\rho_\pi \propto 1/Q^2$ so that

Beam Polarization

- Beam polarization determined from Moeller measurements taken through the run period.
- Su22: 83.84 +/- 0.86%
- Fa22: 83.72 +/- 0.45%
- Sp23: 80.40 +/- 0.61%

```
run number, data, polarization percentage, statistical uncertainty percentage, logbook link
only Moeller runs with charge asymmetry <2%; Hall C bleed through runs removed, adjusted Wien angles removed

RGC Su22 Inb, runs 16043-16772
140, 06/25/2022, 83.893, 1.473, https://logbooks.jlab.org/entry/4007315
163, 08/15/2022, 83.005, 1.494, https://logbooks.jlab.org/entry/4029289
164, 08/24/2022, 84.630, 1.490, https://logbooks.jlab.org/entry/4033346
Weighted Mean: 83.84 +/- 0.86(stat) +/- 0.81(sys from std); combine with 2% scale sys:
83.84 +/- 0.86(stat) +/- 2.16(sys)

RGC Fa22 Inb, runs 16843-17408
167, 09/14/2022, 86.187, 1.209, https://logbooks.jlab.org/entry/4041675
169, 09/26/2022, 81.346, 1.477, https://logbooks.jlab.org/entry/4047006
171, 10/09/2022, 87.004, 1.451, https://logbooks.jlab.org/entry/4052619
173, 10/14/2022, 82.698, 1.256, https://logbooks.jlab.org/entry/4059176
174, 10/14/2022, 80.948, 1.416, https://logbooks.jlab.org/entry/4059208
175, 10/17,2022, 84.373, 1.463, https://logbooks.jlab.org/entry/4061436
176, 10/23/2022, 82.529, 1.234, https://logbooks.jlab.org/entry/4066556
177, 10/27,2022, 85.137, 1.401, https://logbooks.jlab.org/entry/4071349
178, 11/02/2022, 83.076, 1.345, https://logbooks.jlab.org/entry/4075558
Weighted Mean: 83.72 +/- 0.45(stat) +/- 2.11(sys from std); combine with 2% scale sys:
83.72 +/- 0.45(stat) +/- 2.91(sys)

RGC Sp23 Inb, runs 17477-17811
180, 02/08/2023, 83.294, 1.494, https://logbooks.jlab.org/entry/4127008
181, 02/25/2023, 77.972, 1.464, https://logbooks.jlab.org/entry/4138705
182, 02/27,2023, 79.780, 2.280, https://logbooks.jlab.org/entry/4140187
183, 02/27/2023, 84.203, 1.499, https://logbooks.jlab.org/entry/4140437
184, 02/27/2023, 71.528, 2.097, https://logbooks.jlab.org/entry/4140449
187, 03/06/2023, 79.407, 1.492, https://logbooks.jlab.org/entry/4144176
188, 03/15/2023, 81.987, 1.476, https://logbooks.jlab.org/entry/4150249
Weighted Mean: 80.40 +/- 0.61(stat) +/- 4.25(sys from std); combine with 2% scale sys:
80.40 +/- 0.61(stat) +/- 4.70(sys)
```

Target Polarization

- N. Pilleux Wiki for elastic analysis for $P_b P_t$ extraction.
- Elastic analysis leveraging the known A_{LL} in order to determine P_t.
- Two separate DIS analyses have been performed and found to be largely consistent.

$$P_b \times P_t = \frac{\sum_{i=0}^{N_{bins}} f_i A_{th,i}(N_i^+ - N_i^-)}{\sum_{i=0}^{N_{bins}} f_i^2 A_{th,i}^2 (N_i^+ + N_i^-)}$$

$$\Delta^2_{P_b \times P_t} = \frac{\sum_{i=0}^{N_{bins}} (f_i A_{th,i})^2 (\frac{N_i^+}{FC^+} + \frac{N_i^-}{FC^-})}{(\sum_{i=0}^{N_{bins}} (f_i A_{th,i})^2 (N_i^+ + N_i^-))^2}$$

Run Period	Positive P_t	Negative P_t
RGC Su22	0.847 ± 0.037	-0.788 ± 0.037
RGC Fa22	0.848 ± 0.024	-0.836 ± 0.024
RGC Sp23	0.833 ± 0.038	-0.771 ± 0.038

- $9.5 < E_{beam}^{calc} < 11.3GeV$
- $-0.05 < MM_{ep}^2 < 0.05GeV^2$
- $178 < |\Phi_e - \Phi p| < 181°$
- $-0.5 < dP_p < 0.56GeV/c$
- $-0.5 < dP_e < 0.5GeV/c$ (difference between the expected and measured e momenta)

exclusivity selection

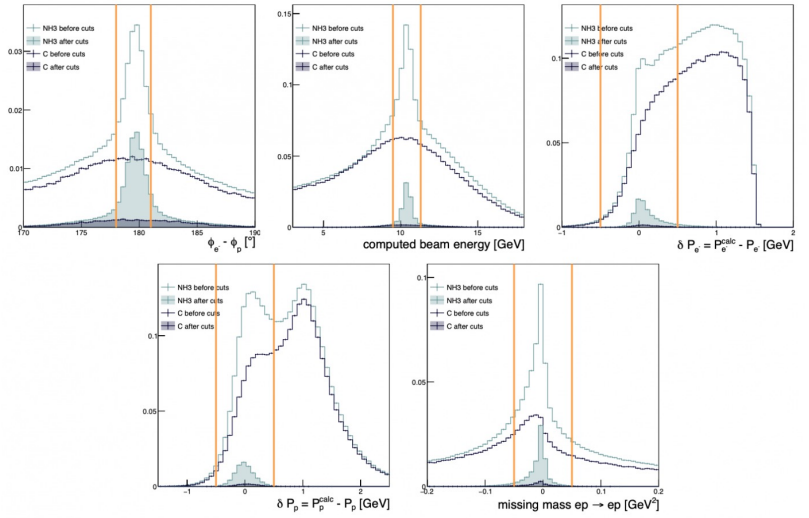

Depolarization Factors

$$A(\epsilon,y) \equiv \frac{y^2}{2(1-\epsilon)} = \frac{1}{1+\gamma^2}\left(1-y+\frac{1}{2}y^2+\frac{1}{4}\gamma^2y^2\right) \approx \left(1-y+\frac{1}{2}y^2\right),$$

$$B(\epsilon,y) \equiv \frac{y^2}{2(1-\epsilon)}\epsilon = \frac{1}{1+\gamma^2}\left(1-y-\frac{1}{4}\gamma^2y^2\right) \approx (1-y),$$

$$C(\epsilon,y) \equiv \frac{y^2}{2\,(1-\epsilon)}\sqrt{1-\epsilon^2} = \frac{y}{\sqrt{1+\gamma^2}}\left(1-\frac{1}{2}y\right) \approx y\left(1-\frac{1}{2}y\right),$$

$$V(\epsilon,y) \equiv \frac{y^2}{2\,(1-\epsilon)}\sqrt{2\epsilon(1+\epsilon)} = \frac{2-y}{1+\gamma^2}\sqrt{1-y-\frac{1}{4}\gamma^2y^2} \approx (2-y)\sqrt{1-y},$$

$$W(\epsilon,y) \equiv \frac{y^2}{2\,(1-\epsilon)}\sqrt{2\epsilon(1-\epsilon)} = \frac{y}{\sqrt{1+\gamma^2}}\sqrt{1-y-\frac{1}{4}\gamma^2y^2} \approx y\sqrt{1-y},$$

A. Bacchetta et al., JHEP, vol. 02, p. 093, 2007.

$$A_{LU}^{\sin\phi} = \left(\frac{W}{A}\right)\left(\frac{F_{LU}^{\sin\phi}}{F_{UU}}\right),$$

$$A_{UL}^{\sin\phi} = \left(\frac{V}{A}\right)\left(\frac{F_{UL}^{\sin\phi}}{F_{UU}}\right), \quad A_{UL}^{\sin 2\phi} = \left(\frac{B}{A}\right)\left(\frac{F_{UL}^{\sin 2\phi}}{F_{UU}}\right),$$

$$A_{LL} = \left(\frac{C}{A}\right)\left(\frac{F_{LL}}{F_{UU}}\right), \quad A_{LL}^{\cos\phi} = \left(\frac{W}{A}\right)\left(\frac{F_{LL}^{\cos\phi}}{F_{UU}}\right),$$

$$A_{UU}^{\cos\phi} = \left(\frac{V}{A}\right)\left(\frac{F_{UU}^{\cos\phi}}{F_{UU}}\right), \quad A_{UU}^{\cos 2\phi} = \left(\frac{B}{A}\right)\left(\frac{F_{UU}^{\cos 2\phi}}{F_{UU}}\right)$$

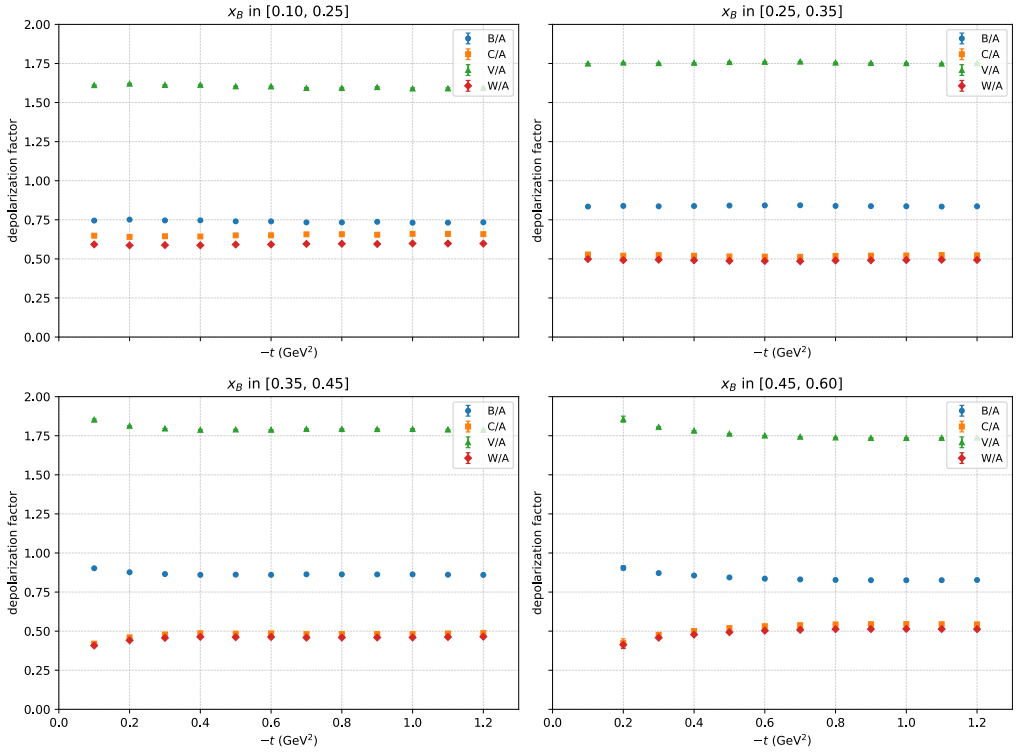

Nearly constant in –t.

Exclusive Final State

Each x_B-t bin's M_x^2 distribution is fit individually to determine cuts.

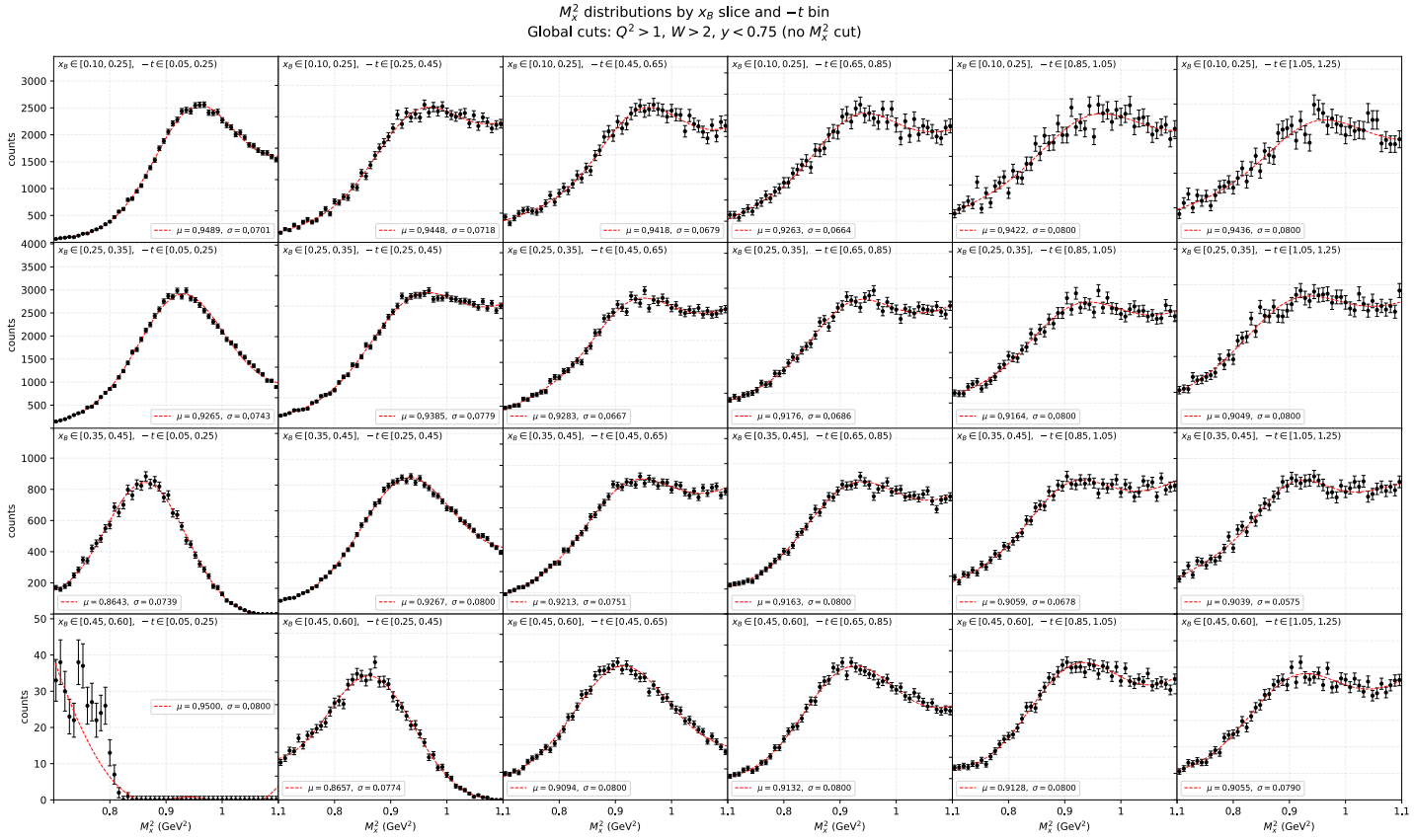

Independence of solenoid setting

- RGC Fa22 data with both solenoid settings were investigated separately in each bin and found to return consistent asymmetries.

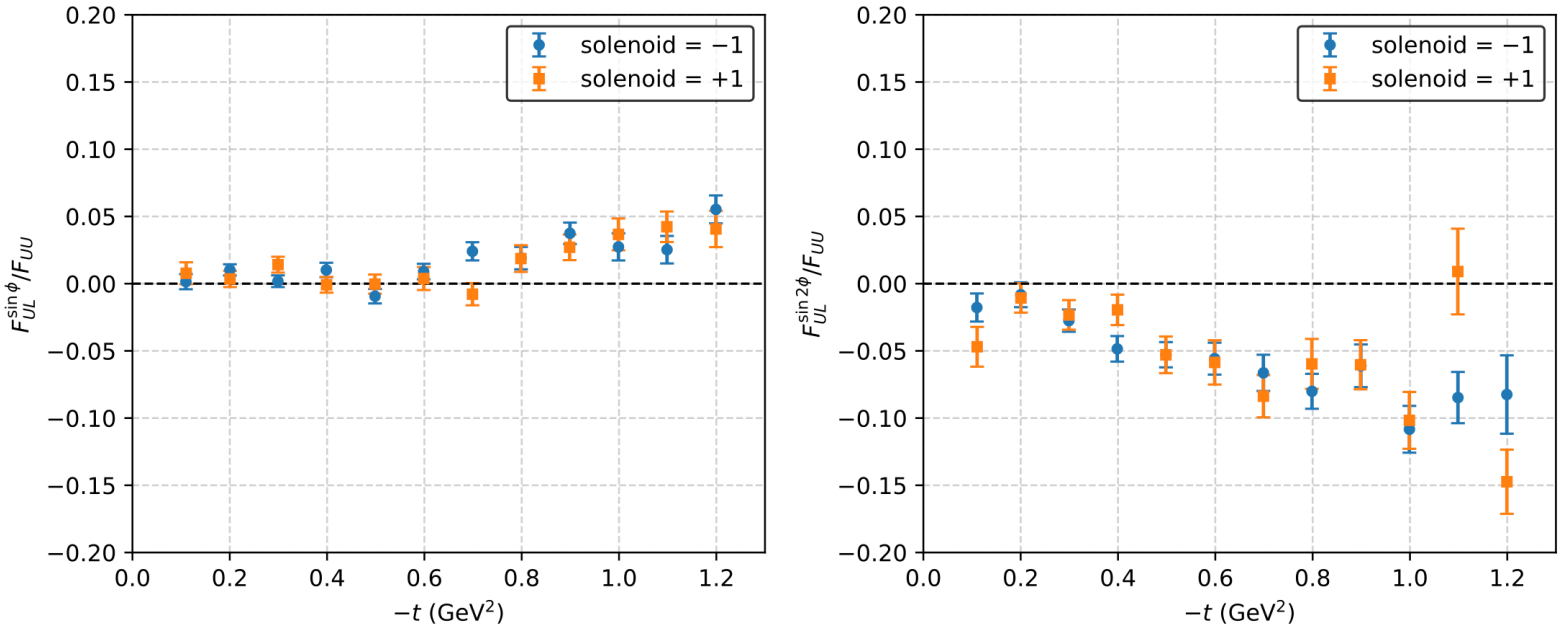

Acceptance Related Effects

- Non-vanishing mean sin(nϕ) indicates possible acceptance related effects.
- Unfolding the data yields with the clasdis MC does not remove these effects (whether because the solenoid “kick” is not fully reflected in MC or because clasdis does not model the exclusive π^+ channel very well).
- Effect is greatly enhanced at lower -t and largely disappears above -t = 1.

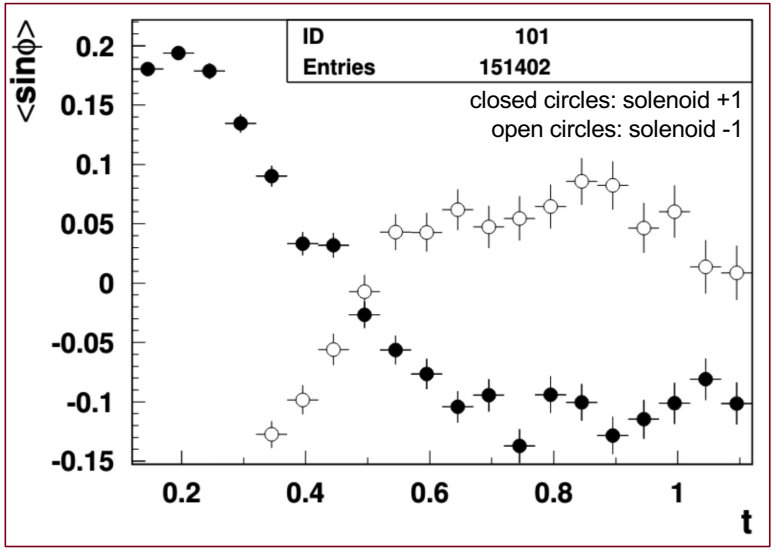

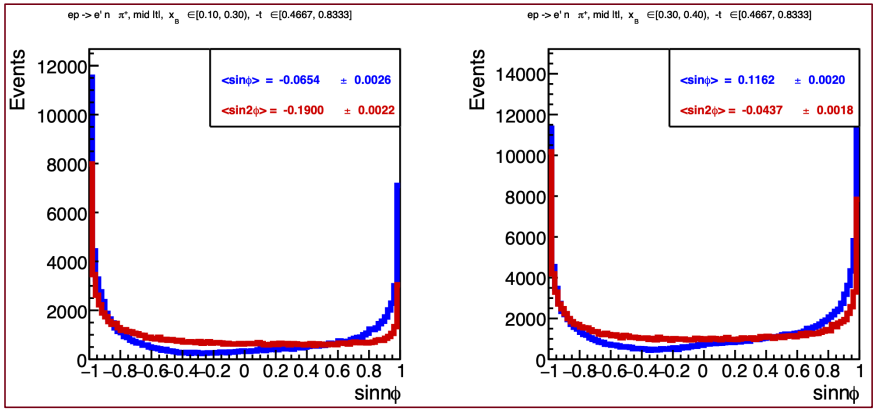

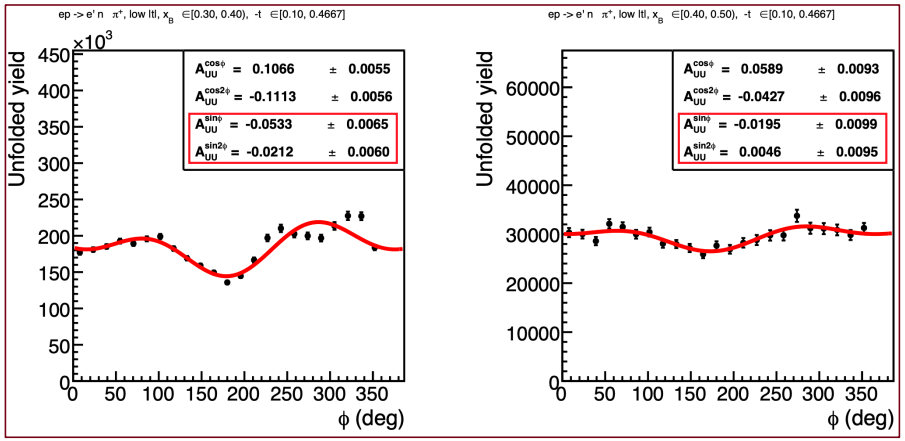

Stability of F_{LU} structure function

1. Extracted from RGA Fa18 Inb data with no unpolarized modulations.
2. Extracted from RGA Fa18 Inb data with the unpolarized $\cos\phi$ and $\cos 2\phi$ modulations included in the fit function.
3. Extracted from RGA Fa18 Inb data with the unpolarized $\cos\phi$ and $\cos 2\phi$ amplitudes fixed to the values extracted from an unfolding of the MC data.
4. Extracted from RGC Fa22 Inb Carbon data with no unpolarizedm odulations.
5. Extracted From RGC Fa22 Inb Carbon data with $\cos\phi$ and $\cos 2\phi$ modulations included in the fit function.
6. Extracted from RGC Fa22 Inb Carbon data with the $\cos\phi$ and $\cos 2\phi$ amplitudes fixed to the values extracted from an unfolding of the MC data.

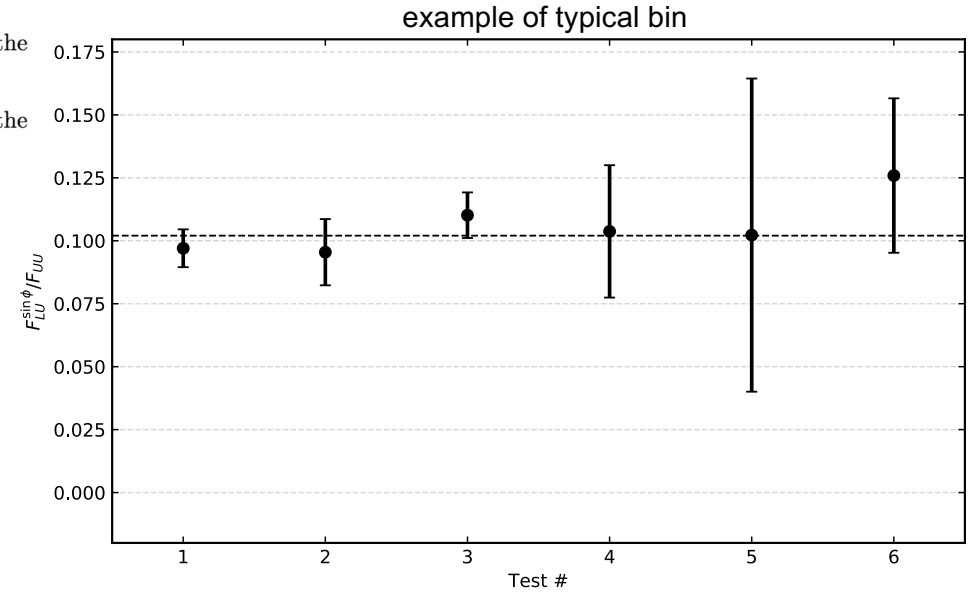

Stability of F_{UL} and F_{LL} structure functions

1. Extracted from RGC Fa22 NH_3 data with all polarized modulations but no unpolarized modulations included in the fit.
2. Extracted from RGC Fa22 NH_3 data with all polarized modulations and $\cos\phi$ and $\cos 2\phi$ unpolarized modulations included in the fit.
3. Extracted from RGC Fa22 NH_3 data with the $F_{LU}^{\sin\phi}$, $F_{UU}^{\cos\phi}$ and $F_{UU}^{\cos 2\phi}$ modulations fixed to values extracted from an independent fit to RGA data in the same kinematic bin.
4. Extracted from RGC Fa22 NH_3 data with the $F_{LU}^{\sin\phi}$ amplitude fixed by an independent fit to RGA data and the $F_{UU}^{\cos\phi}$ and $F_{UU}^{\cos 2\phi}$ modulations fixed to the values extracted from an unfolding of the MC data.
5. Extracted from RGC Fa22 NH_3 data with all polarized and unpolarized modulations allowed to float including two unpolarized sine modulations $A_{UU}^{\sin\phi}$ and $A_{UU}^{\sin 2\phi}$.

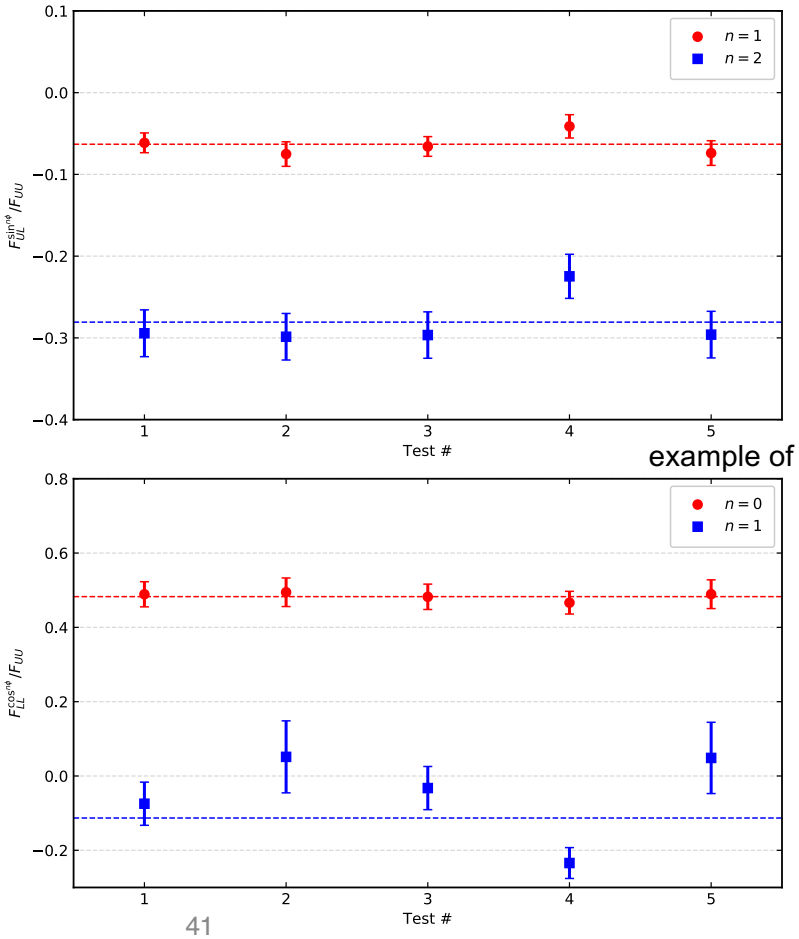

example of typical bin

Binned Results (Requested For Release)

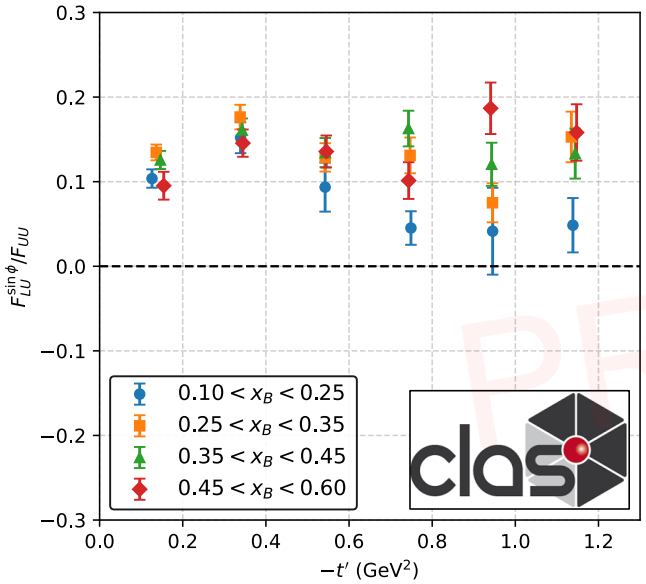

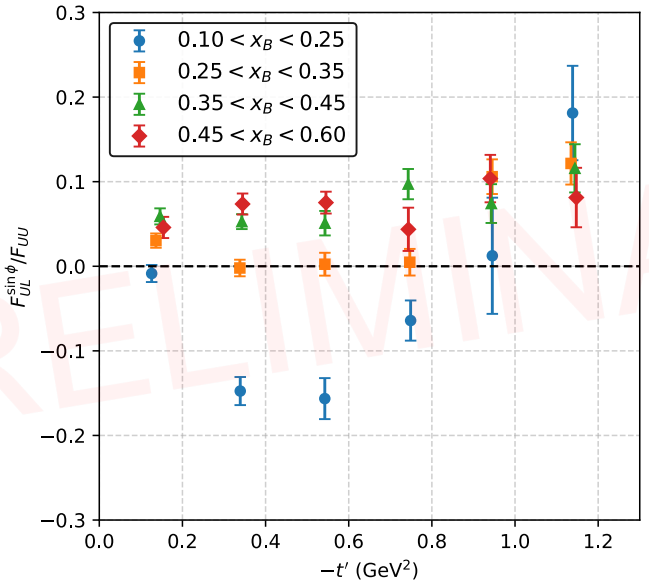

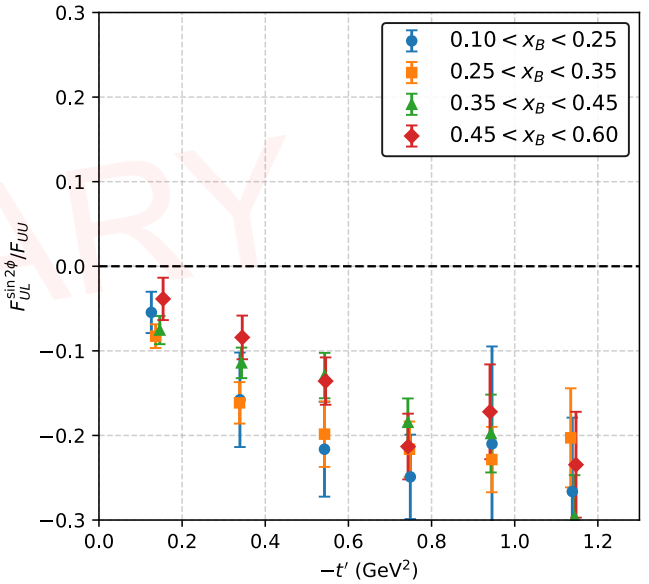

Integrated Asymmetry (Requested For Release)